8 Microphysical Processes in Warm Clouds

Warm clouds are clouds that do not contain any ice. Nevertheless, their cloud tops may still extend to altitudes where temperatures are below the melting point of water. In the absence of ice, this is an environment in which supercooled cloud droplets can exist in a thermodynamically metastable state (Section 3.4.5). In Chapter 7, we discussed how aqueous solution droplets are activated into cloud droplets. During the entire growth process, the droplet grows by uptaking water molecules from the supersaturated vapor phase. Water vapor molecules are transported via diffusion toward the droplet surface where condensation takes place. This process is called diffusional or condensational growth (Section 8.1). Additional processes involving collisions with other droplets are required for the droplets to reach precipitation size (Table 1.2), since diffusion of water vapor alone is often too slow to produce precipitation-sized drops on the time scales observed in the atmosphere. This growth is referred to as growth by collision-coalescence (Section 8.2). Coalescence is a special case of coagulation that involves two liquid hydrometeors. Evaporation and break-up of raindrops, which limits raindrops to a maximum radius of around 5 mm, are discussed in Section 8.3. Note that here we distinguish between *droplets*, which are small enough to have negligible fall speeds, for example, cloud droplets, and *drops* that have appreciable fall velocities, such as drizzle drops and raindrops.

Figure 8.1 shows typical sizes for a CCN, a cloud droplet, a drizzle drop, and a raindrop, along with their typical concentrations exemplary for the marine atmosphere: typical marine CCN number concentrations range between 10^2 and 10^3 cm^{-3} while a typical number concentration for cloud droplets over ocean is $10^2\,cm^{-3}$ (Kubar et al., 2009). This shows that for typical environmental supersaturations (s_w from 0.1 to 1.6 %) (Hudson et al., 2010, 2015), not all aerosol particles become activated into cloud droplets (Chapter 7).

After activation, a cloud droplet must grow one order of magnitude in radius in order to reach the size of a drizzle drop of a typical radius of 0.05 mm (Table 1.2 and Sant et al. (2013)). Put differently, it requires the water of a thousand cloud droplets to form a single drizzle drop. Their typical number concentration in marine clouds is $0.1\,cm^{-3}$, which is about three orders of magnitude smaller than that of cloud droplets (Wood et al., 2009) and about three orders of magnitude larger than that of raindrops with $10^{-4}\,cm^{-3}$ ($100\,m^{-3}$) and a typical radius of 0.5 mm. Raindrops are large enough to have fall velocities that overcome the updraft speeds within a cloud and hence fall out of the cloud as precipitation.

https://doi.org/10.1017/9781009485654.009 Published online by Cambridge University Press

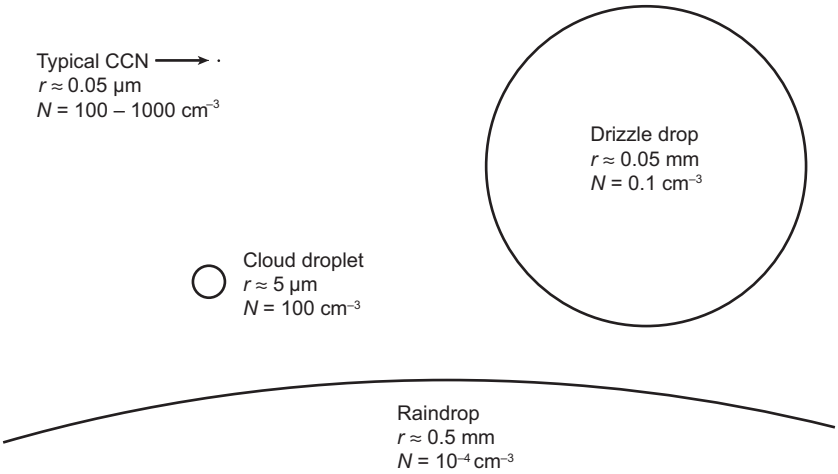


Figure 8.1 Comparative sizes and concentrations of the particles involved in a typical marine cloud and precipitation processes (Table 1.2).

8.1 Droplet Growth by Diffusion and Condensation

As discussed in Chapter 7 and shown in Figure 8.2, an aqueous solution droplet can spontaneously grow into a cloud droplet in an environment in which $S_w > S_{act}$. Now we will discuss this growth in more detail. Note that *condensational growth* specifically indicates diffusional growth of droplets within a gas phase that is supersaturated with respect to water vapor. By contrast, *diffusional growth* more broadly includes growth by water vapor uptake of all hydrometeors in sub- and supersaturated environments. Before reaching r_{act}, the solution droplet grows in equilibrium with the environmental saturation ratio S_{env}. Once r_{act} is reached, the droplet grows spontaneously and continues to grow as long as $S(r) < S_{env}$ (Section 7.5.1 and Figures 8.2 and 7.13). The droplet growth equation can be obtained from a combination of the diffusion equations for water vapor and heat, as will be discussed in the following.

8.1.1 Diffusion Equation for Water Vapor

The diffusion equation for water vapor is given as

$$\frac{\partial n_v}{\partial t} = D_v \nabla^2 n_v = D_v \Delta n_v, \tag{8.1}$$

where n_v is the number concentration of water vapor molecules and D_v is the diffusivity (or diffusion rate) for any concentration gradient; here evaluated for water vapor in air. Equation (8.1) is also called Fick's second law of diffusion (Fick, 1855). Fick's laws postulate that in the presence of a concentration gradient the diffusion flux J in units of amount of substance n per unit area and unit time is directed from regions of high concentration to regions of low concentration, with the magnitude proportional to the concentration gradient:

$$\vec{J} = -D \nabla n, \tag{8.2}$$

where D is the general diffusivity.

https://doi.org/10.1017/9781009485654.009 Published online by Cambridge University Press

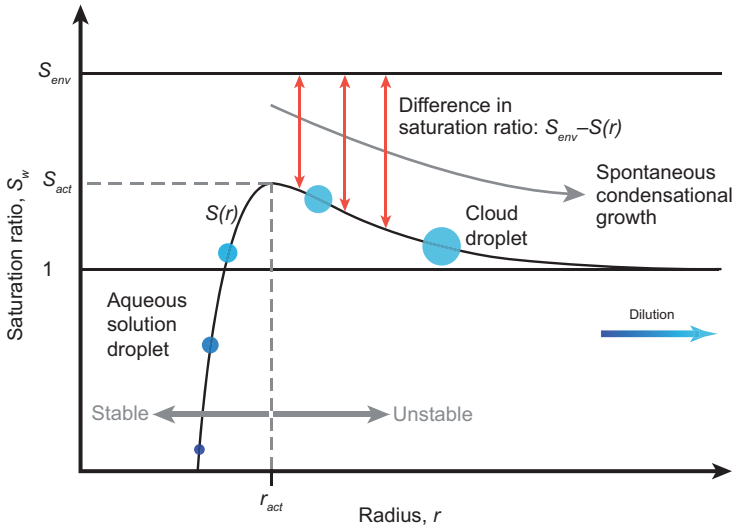


Figure 8.2 Schematic of the condensational growth process for a cloud droplet at a given environmental saturation ratio S_{env} after Köhler activation at r_{act}. The condensational growth process is driven by the difference $S_{env} - S(r)$.

We now place a droplet with radius r_d inside a continuous vapor field and assume that the concentration of water molecules at a radial distance r away from the droplet is $n_v(r)$. We assume that the water vapor field is isotropic (uniform in all directions) around the droplet all the way up to the droplet's surface. In such a case, it is advantageous to use spherical coordinates (r, θ, φ) because the derivatives with respect to θ and φ are zero. Furthermore, we assume steady-state conditions, which means that the time dependence of the variable of interest is zero (i.e., $\partial n_v / \partial t = 0$), and that the sources and sinks exactly balance each other. Then, eq. (8.1) can be written in spherical coordinates as follows:

$$D_v \Delta n_v = D_v \frac{1}{r^2} \frac{\partial}{\partial r} \left(r^2 \frac{\partial n_v}{\partial r} \right) = 0, \tag{8.3}$$

with the general solution:

$$n_v(r) = C_1 - \frac{C_2}{r}, \tag{8.4}$$

where C_1 and C_2 are constants of integration. The water vapor field has the following boundary conditions: For $r \to \infty$, the vapor concentration n_v approaches $n_{v,\infty}$, the undisturbed water vapor concentration far from the droplet surface. For $r \to r_d$, the vapor concentration n_v approaches n_{v,r_d}, the water vapor concentration at the surface of a droplet with $r = r_d$.

This yields the special solution

$$n_v(r) = n_{v,\infty} - \frac{r_d}{r}(n_{v,\infty} - n_{v,r_d}), \tag{8.5}$$

https://doi.org/10.1017/9781009485654.009 Published online by Cambridge University Press

with the gradient of the vapor concentration given as

$$\frac{\partial n_v}{\partial r} = \frac{r_d}{r^2}(n_{v,\infty} - n_{v,r_d}). \tag{8.6}$$

The gradient in the water vapor concentration between the environment far from the droplet and near the droplet's surface causes a diffusive flux of water vapor. In a supersaturated environment, the flux is directed toward the droplet, where the molecules condense on the surface and cause the droplet to grow. From eq. (8.6), we see that the gradient scales with $1/r^2$; hence, it is small at large radial distances away from the droplet and large close to the droplet surface, where it maximizes. We evaluate eq. (8.6) at the droplet surface $r = r_d$:

$$\left(\frac{\partial n_v}{\partial r}\right)_{r=r_d} = \frac{1}{r_d}(n_{v,\infty} - n_{v,r_d}). \tag{8.7}$$

Similarly, we obtain the flux density of water vapor molecules condensing onto the surface of the droplet as $D_v\,(\partial n_v/\partial r)_{r=r_d}$. This leads to the following rate of droplet mass increase due to diffusional growth:

$$\frac{dm_l}{dt} = 4\pi r_d^2 D_v \left(\frac{\partial n_v}{\partial r}\right)_{r=r_d} m_0, \tag{8.8}$$

where m_0 denotes the mass of one water molecule (3×10^{-26} kg). Inserting eq. (8.7) into eq. (8.8) yields

$$\frac{dm_l}{dt} = 4\pi r_d D_v (n_{v,\infty} - n_{v,r_d}) m_0. \tag{8.9}$$

Thus, the rate of mass increase depends linearly on the droplet radius. Replacing $n_{v,r_d}m_0$ by the water vapor density ρ_{v,r_d} at the droplet surface (r_d) and $n_{v,\infty}m_0$ by the environmental water vapor density ρ_v yields

$$\frac{dm_l}{dt} = 4\pi r_d D_v (\rho_v - \rho_{v,r_d}). \tag{8.10}$$

Equation (8.10) is the diffusional growth equation for an isolated droplet at rest. It shows that the droplet grows if $\rho_v > \rho_{v,r_d}$ and evaporates if $\rho_v < \rho_{v,r_d}$. ρ_v is available from ambient measurements, but ρ_{v,r_d} depends on the droplet size, chemical composition, and temperature.

8.1.2 Heat Conduction Equation

The temperature at the droplet surface considering latent heat release or consumption is not the same as the environmental temperature so the heat transfer between the droplet and the environment needs to be considered as well. The equations of mass and heat fluxes were first derived in 1877 by James Clerk Maxwell[1]. Thus, the steady-state growth of spherical water droplets at rest in a continuous water vapor field is often referred to as Maxwell's growth theory.

Condensation leads to an increase in droplet temperature owing to the release of latent heat (Figure 8.3a). This has considerable implications for the parameters that determine droplet growth. Certainly, an increase in droplet temperature causes the saturation water vapor

[1] www.britannica.com/biography/James-Clerk-Maxwell

https://doi.org/10.1017/9781009485654.009 Published online by Cambridge University Press

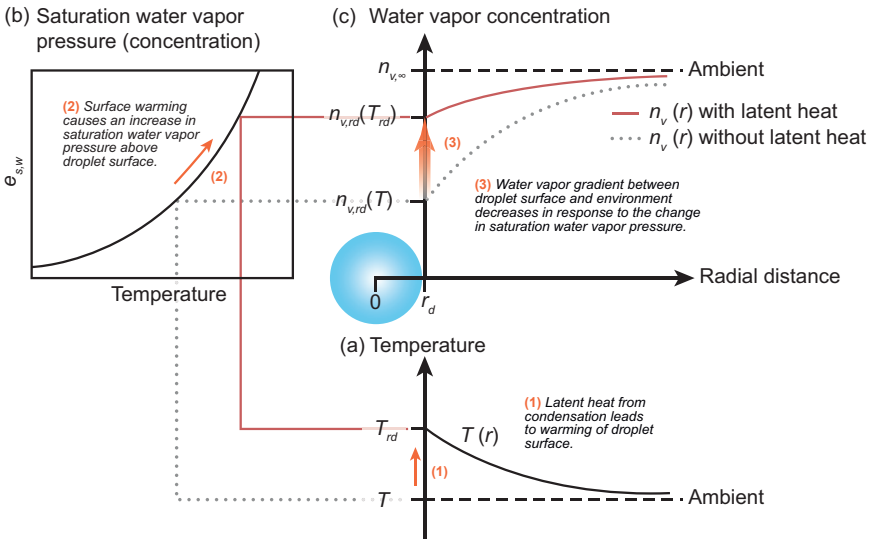


Figure 8.3 Schematic of the effect of latent heat release on the condensational growth process of a cloud droplet, which is at rest in an environment that is supersaturated with respect to liquid water. Release of latent heat due to condensation affects the temperature of the droplet (a), which in turn affects the saturation water vapor pressure above the droplet, as given by the Clausius–Clapeyron equation (3.70) (b), ultimately resulting in a change in the water vapor concentration above the droplet (c).

pressure at the droplet surface to increase (Figure 8.3b). Since the water vapor pressure at the droplet surface equals its saturation vapor pressure according to the Clausius–Clapeyron equation (eq. 3.70), the water vapor pressure gradient between the supersaturated environment and the droplet surface decreases as shown in Figure 8.3c. This means that neglecting the latent heat release would cause an overestimation of the condensational growth rate of cloud droplets.

The latent heat release due to condensation can be taken into account by evaluating the rate of heat transfer dQ_c/dt from the droplet, which is given by the heat conduction equation. This equation is analogous to the vapor diffusion equation (eq. 8.10), again evaluated at the droplet's surface:

$$\frac{dQ_c}{dt} = -4\pi r K(T - T_{r_d}), \tag{8.11}$$

where T is the environmental temperature far away from the droplet, T_{r_d} is the temperature at the droplet surface, K is the thermal conductivity in air and Q_c is the heat due to conduction. The heat conduction equation is based on the studies of the French mathematician Jean-Baptiste Joseph Fourier[2] on heat transfer in solid bodies and fluids (Fourier, 1822, 2009). Fourier's law of conduction states that in the presence of a temperature gradient, an energy flux is transported down the gradient.

[2] www.britannica.com/biography/Joseph-Baron-Fourier

https://doi.org/10.1017/9781009485654.009 Published online by Cambridge University Press

8.1.3 Droplet Growth Equation

To obtain an expression for the rate of change of the temperature at the surface of a water droplet, both vapor diffusion and heat conduction need to be taken into account. From the first law of thermodynamics, the change in the surface temperature of the droplet is given by

$$m_l c_l \frac{dT_{r_d}}{dt} = \frac{dq}{dt}, \tag{8.12}$$

where m_l is the mass of the droplet and c_l is the specific heat capacity of liquid water (eq. A.8). Note that dq is the total heat transfer while dQ_c (eq. 8.11) refers only to heat conduction. Thus, dq/dt comprises the heat transfer due to latent heat release plus that due to the conduction of heat, so that

$$m_l c_l \frac{dT_{r_d}}{dt} = L_v \frac{dm_l}{dt} - \frac{dQ_c}{dt}. \tag{8.13}$$

We assume a steady state, in which the diffusion of water vapor to the droplet with its associated latent heat release upon condensation onto the droplet surface is exactly balanced by the heat conduction away from the droplet, so that $dT_{r_d}/dt = 0$. Replacing the expressions for dm_l/dt and dQ_c/dt with eqs. (8.10) and (8.11), respectively, yields

$$4\pi r K(T_{r_d} - T) = 4\pi r D_v(\rho_v - \rho_{v,r_d})L_v. \tag{8.14}$$

After rearranging terms, we obtain

$$\frac{K}{D_v L_v} = \frac{\rho_v - \rho_{v,r_d}}{T_{r_d} - T}. \tag{8.15}$$

In eq. (8.15), ρ_{v,r_d} and T_{r_d} are unknown. They are related by the Köhler equation (7.30). Using the ideal gas law for water vapor (eq. 3.11) allows us to express the Köhler equation in terms of ρ_{v,r_d}:

$$\rho_{v,r_d} = \frac{e^*(r)}{R_v T_{r_d}} = \left(1 + \frac{a}{r} - \frac{b}{r^3}\right) \frac{e_{s,w}(T_{r_d})}{R_v T_{r_d}}, \tag{8.16}$$

where $e^*(r)$ refers to the equilibrium water vapor pressure over an aqueous solution droplet (Chapter 7). $e_{s,w}(T_{r_d})$ denotes the saturation water vapor pressure over a flat (bulk) water surface, which can be obtained from the Clausius–Clapeyron equation (3.70). Equations (8.15) and (8.16) comprise a coupled set of equations, which can only be solved numerically.

An analytical approximation of the droplet growth equation is possible, as described by Mason (1971), if the solute and curvature terms of the Köhler equation are ignored. Since the solute and curvature effects are small for droplets larger than a few micrometers (Figure 7.11), this assumption is justified at droplet sizes beyond cloud droplet activation (see eq. 8.30 for the complete equation). Using the Clausius–Clapeyron equation (3.70) in conjunction with the ideal gas law for water vapor (eq. 3.11) yields the change in saturation water vapor density ρ_{vs} with temperature:

$$\frac{d\rho_{vs}}{\rho_{vs}} = \frac{L_v}{R_v}\frac{dT}{T^2} - \frac{dT}{T}. \tag{8.17}$$

https://doi.org/10.1017/9781009485654.009 Published online by Cambridge University Press

Integrating from T_{r_d} to T gives

$$\ln \frac{\rho_{vs}}{\rho_{vs,r_d}} = (T - T_{r_d}) \left(\frac{L_v}{R_v T_{r_d} T} \right) - \ln \frac{T}{T_{r_d}}. \tag{8.18}$$

Assuming that $\rho_{vs}/\rho_{vs,r_d} \approx 1$ and $T/T_{r_d} \approx 1$, we can use a Taylor series to approximate $\ln \rho_{vs}/\rho_{vs,r_d}$ as $\rho_{vs}/\rho_{vs,r_d} - 1$ and $\ln T/T_{r_d}$ as $T/T_{r_d} - 1$. Further assuming that $T \cdot T_{r_d} \approx T^2$ yields:

$$\frac{\rho_{vs} - \rho_{vs,r_d}}{\rho_{vs,r_d}} \approx \left(\frac{T - T_{r_d}}{T} \right) \left(\frac{L_v}{R_v T} - 1 \right). \tag{8.19}$$

We can then use eq. (8.11) to replace $T - T_{r_d}$, and use the steady-state version of eq. (8.13) to replace dQ_c/dt with $L_v dm_l/dt$ to obtain:

$$\frac{\rho_{vs} - \rho_{vs,r_d}}{\rho_{vs,r_d}} = -\frac{dm_l}{dt} \left(\frac{L_v}{4\pi r K T} \right) \left(\frac{L_v}{R_v T} - 1 \right). \tag{8.20}$$

To include this expression in the diffusional growth equation, we divide eq. (8.10) by ρ_{vs,r_d}:

$$\frac{\rho_v - \rho_{v,r_d}}{\rho_{vs,r_d}} = \frac{dm_l}{dt} \left(\frac{1}{4\pi r D_v \rho_{vs,r_d}} \right). \tag{8.21}$$

If we then assume that the water vapor density at the droplet's surface equals the saturated water vapor density ($\rho_{v,r_d} = \rho_{vs,r_d}$) and approximate ρ_{vs,r_d} in the denominator as ρ_{vs}, and finally subtract eq. (8.20) from the expression in eq. (8.21), we obtain:

$$\frac{\rho_v - \rho_{vs}}{\rho_{vs}} = \frac{dm_l}{dt} \left[\left(\frac{1}{4\pi r D_v \rho_{vs}} \right) + \frac{L_v}{4\pi r K T} \left(\frac{L_v}{R_v T} - 1 \right) \right]. \tag{8.22}$$

Now, the final step is to replace ρ_v/ρ_{vs} by the water saturation ratio S_w and re-arrange the terms to obtain the mass growth equation by condensation for a cloud droplet:

$$\frac{dm_l}{dt} = 4\pi r \frac{S_w - 1}{\frac{L_v}{KT} \left(\frac{L_v}{R_v T} - 1 \right) + \frac{1}{D_v \rho_{vs}}} = 4\pi r \frac{S_w - 1}{F_k^l + F_d^l}. \tag{8.23}$$

The previously mentioned equation is also known as *Maxwell's mass growth equation of cloud droplets*. F_k^l (units of $\mathrm{m\,s\,kg^{-1}}$) is the thermodynamic term related to the latent heat release due to the condensation and diffusion of heat away from the droplet, whereas F_d^l (also in units of $\mathrm{m\,s\,kg^{-1}}$) is the water vapor diffusion term, related to the diffusion of water vapor molecules to the droplet's surface.

The term F_k^l depends on the environmental temperature T, the latent heat of vaporization L_v, and the thermal conductivity K, and is given as:

$$F_k^l = \left(\frac{L_v}{R_v T} - 1 \right) \frac{L_v}{KT} \approx \left(\frac{L_v^2}{K R_v T^2} \right). \tag{8.24}$$

K is only weakly dependent on pressure (Kadoya et al., 1985), but increases noticeably with increasing temperature. This is due to the higher kinetic energy of the air molecules at higher temperatures causing faster heat conduction. For dry air, the temperature dependence of K

https://doi.org/10.1017/9781009485654.009 Published online by Cambridge University Press

in units $\mathrm{J\,m^{-1}\,s^{-1}\,K^{-1}}$ can be approximated by an empirical relation based on Beard and Pruppacher (1971):

$$K = 4.1868 \times 10^{-3}\,[5.69 + 0.0168(T - T_0)], \tag{8.25}$$

where $T_0 = 273.15\,\mathrm{K}$. This expression for the thermal conductivity is based on measurements of Taylor and Johnston (1946), who measured K between 87 and 375 K. For typical atmospheric conditions, the volume fraction of water vapor in moist air is small (below 4 %), allowing us to approximate the thermal conductivity of moist air by that for dry air (eq. 8.25).

The term F_d^l depends on the saturation water vapor pressure, temperature, and the water vapor diffusivity in air, D_v:

$$F_d^l = \frac{1}{D_v \rho_{vs}} = \frac{R_v T}{D_v e_{s,w}(T)}. \tag{8.26}$$

D_v increases with increasing temperature but decreases with increasing atmospheric pressure: an increase in atmospheric pressure means a decrease in the mean free path λ_a of molecules in air, so that random collisions with other molecules and particles occur more frequently. λ_a is given as:

$$\lambda_a = \lambda_{a,0} \left(\frac{p_{0,\lambda}}{p}\right) \left(\frac{T}{T_{0,\lambda}}\right) \tag{8.27}$$

where $\lambda_{a,0} = 6.6 \times 10^{-8}\,\mathrm{m}$ is obtained at the reference values of $p_{0,\lambda} = 1013.25\,\mathrm{hPa}$ and $T_{0,\lambda} = 293.15\,\mathrm{K}$. The increase in D_v with increasing temperature represents the higher mobility of molecules at higher temperatures. The change in D_v with temperature can be approximated for temperatures between 193.15 and 313.15 K as follows (Hall and Pruppacher, 1976):

$$D_v = 2.11 \times 10^{-5} \left(\frac{T}{T_0}\right)^{1.94} \left(\frac{p_{0,\lambda}}{p}\right) \mathrm{m^2 s^{-1}}, \tag{8.28}$$

with $p_{0,\lambda}$ as defined earlier. Some values of K and D_v for various temperatures and pressures are listed in Table 8.1.

Table 8.1 Values for the thermal conductivity of dry air K in $\mathrm{J\,m^{-1}\,s^{-1}\,K^{-1}}$ according to eq. (8.25) and the diffusion coefficient for water vapor in air D_v in $10^{-5}\,\mathrm{m^2\,s^{-1}}$ according to eq. (8.28). Values are given as a function of temperature in units of K for the indicated pressure values. Also tabulated are values of the dynamic viscosity in air μ in $10^{-5}\,\mathrm{kg\,m^{-1}\,s^{-1}}$ according to eq. (A.10) from Dixon (2007), as needed in Section 8.2.2.

T	K	D_v	D_v	D_v	D_v	D_v	μ
		(1000 hPa)	(800 hPa)	(600 hPa)	(400 hPa)	(200 hPa)	
233.15	0.021	1.57	1.97	2.62	3.93	7.86	1.51
253.13	0.022	1.84	2.31	3.07	4.61	9.22	1.62
273.15	0.024	2.14	2.67	3.56	5.34	10.69	1.72
293.15	0.025	2.45	3.07	4.09	6.13	12.26	1.81
313.15	0.027	2.79	3.48	4.64	6.97	13.94	1.91

https://doi.org/10.1017/9781009485654.009 Published online by Cambridge University Press

For the growth of cloud droplets, it is more common to write the droplet growth equation in terms of radius rather than mass. Assuming spherical droplets, the droplet growth equation in terms of radius can be obtained by replacing dm_l/dt by $4\pi r^2 \rho_l dr/dt$ in eq. (8.23) and dividing by $4\pi r \rho_l$:

$$r\frac{dr}{dt} = \frac{S_w - 1}{F_k + F_d}. \tag{8.29}$$

where $F_k = \rho_l F_k^l$, $F_d = \rho_l F_d^l$. For ρ_l, we use the density of pure water (eq. A.1), because the mole fraction of water is much larger than that of the solute in activated cloud droplets (see Chapter 7). To calculate the droplet growth equation at any temperature, standard parameterizations of the temperature-dependent water density can be used, such as those given in eq. (A.1). Equation (8.29) is known as the *simplified droplet growth equation* because it neglects the solute and curvature effects from the Köhler equation on the droplet's equilibrium water vapor pressure, which is justified for droplets larger than a few micrometers. If the Köhler terms are included, then the full droplet radius growth equation is given as

$$r\frac{dr}{dt} = \frac{(S_w - 1) - a/r + b/r^3}{F_k + F_d}. \tag{8.30}$$

Equation (8.30) cannot be solved analytically. However, for most applications, the simple droplet growth equation (eq. 8.29) is sufficient.

8.1.4 Solution of the Droplet Growth Equation

Equation (8.29) can be integrated to show that the cloud droplet radius varies with time according to

$$r(t) = \sqrt{r_0^2 + 2\left(\frac{S_w - 1}{F_k + F_d}\right)t}. \tag{8.31}$$

As can be seen in eqs. (8.24) and (8.26), F_k depends on temperature and F_d depends on temperature and pressure. The higher the temperature, the smaller F_k. The term F_d includes the temperature-dependent terms in both the nominator and denominator. For F_d, the temperature dependence in the denominator dominates, thus F_d also decreases with increasing temperature. Consequently, the denominator in eq. (8.29) is smaller for higher temperatures, that is, at higher temperatures, droplets grow or shrink faster for a given environmental saturation ratio S_w. This occurs for two reasons: at higher temperatures, (i) the diffusion of air and water vapor molecules is more efficient and (ii) the absolute difference in water vapor pressure between the droplet surface and its surroundings is larger for a given S_w, because of the Clausius–Clapeyron equation. Therefore, the water vapor gradient at the droplet surface, which drives the condensational growth or evaporation of the droplet, is larger at higher temperatures (Figure 8.3).

https://doi.org/10.1017/9781009485654.009 Published online by Cambridge University Press

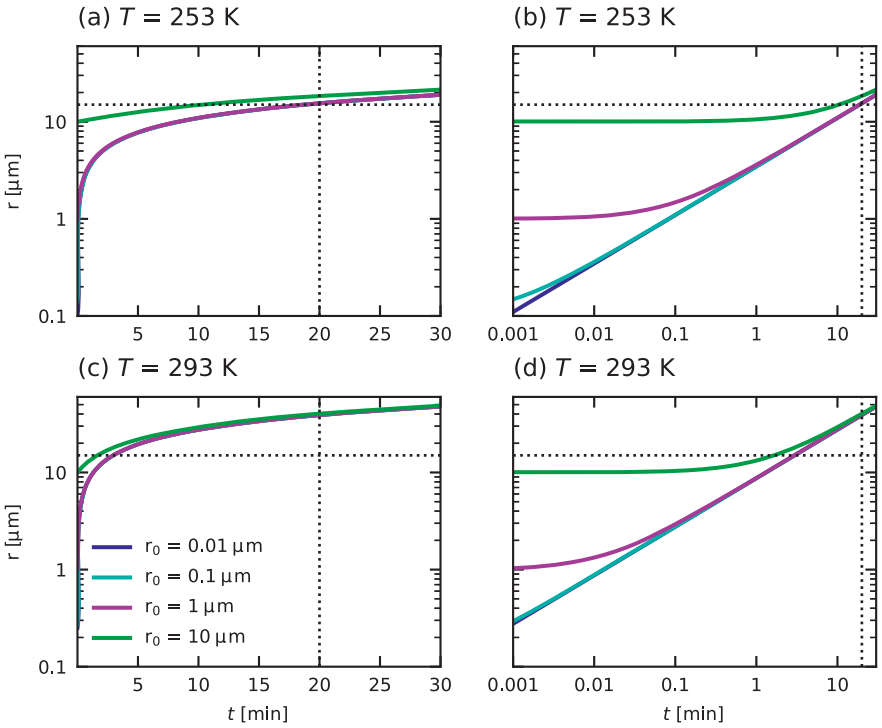


Figure 8.4 Radial droplet growth by diffusion, obtained by evaluating eq. (8.31) for different r_0 values and temperatures plotted (a), (c) on a linear scale and (b), (d) on a logarithmic time scale for $T = 253$ K (a), (b) and for $T = 293$ K (c), (d). The curves were calculated for $S_w = 1.005$ and $p = 800$ hPa. The dotted horizontal lines correspond to a droplet with $r_d = 15$ µm, beyond which collision–coalescence becomes important. 20 min (dotted vertical line) is a typical time for the first observation of precipitation from newly formed cumuli.

Figure 8.4 shows results for the droplet growth equation evaluated for droplets starting at four different initial sizes r_0 and at two different temperatures. It can be seen that the diffusional growth in terms of radius slows down as the droplets become larger. This can be explained by the decrease in surface-to-volume ratio of the larger droplets. As diffusional growth is proportional to the surface area ($\propto r^2$) and mass growth is proportional to the volume ($\propto r^3$), the small droplets, with a larger surface-to-volume ratio, catch up to the larger droplets. This leads to the characteristic parabolic form of eq. (8.31) and to a narrowing of the droplet size distribution as growth proceeds.

Figure 8.4 also illustrates the temperature dependence of droplet growth. It shows that raindrops would not form after 20 min, the typical lifetime of a cumulus cloud (Table 1.3), at an environmental temperature of 253 K, because diffusional growth is too slow. However, at high temperatures ($T = 293$ K in Figure 8.4), at a constant saturation ratio $S_w = 1.005$, diffusional growth is fast enough to produce drizzle drops with radii of 40 µm in 20 min, which corresponds to the timescale observed for rapid rain formation in warm clouds (Saunders, 1965; Stephens and Haynes, 2007). A radius of 15 µm, which is considered the minimum size for

https://doi.org/10.1017/9781009485654.009 Published online by Cambridge University Press

the growth by collision–coalescence (Section 8.2) and thus for the development of rain, can be reached after 3–5 min at an environmental temperature of 293 K.

8.1.5 Growth of a Droplet Population

In reality, droplets within a cloud are not of uniform size and thus start their condensational growth from different sizes. Additionally, the supersaturation does not remain constant but instead will be depleted by condensational growth. Thus, we need to consider the interactions of cloud droplets with the environmental water vapor field and with each other. In the early development of a cloud, the droplets are too small for sedimentation and coalescence to be important. Their initial growth is governed purely by condensational growth. Therefore, we need to examine the vapor budget of a developing cloud. Supersaturation is established in the ascending air parcel owing to adiabatic expansion and cooling of the air ($Q_1 dz/dt$), and is consumed by the condensation of water vapor on the growing cloud droplets ($Q_2 dq_l/dt$). The rate of change of the saturation ratio S_w in an ascending air parcel is thus given by

$$\frac{dS_w}{dt} = Q_1 \frac{dz}{dt} - Q_2 \frac{dq_l}{dt}. \tag{8.32}$$

Here, dz/dt is the vertical velocity w and dq_l/dt is the condensation rate, that is, the mass condensate per unit mass of air and unit time. Q_1 and Q_2 are thermodynamic variables given by

$$Q_1 = \frac{1}{T}\left(\frac{\epsilon L_v g}{R_d c_p T} - \frac{g}{R_d}\right), \tag{8.33}$$

$$Q_2 = \rho_a \left(\frac{R_d T}{\epsilon e_{s,w}} + \frac{\epsilon L_v^2}{p T c_p}\right), \tag{8.34}$$

where ρ_a is the air density. Q_1 has the unit m^{-1} and Q_2 is dimensionless. A detailed derivation of Q_1 and Q_2 is given in Rogers and Yau (1989). The implications of eq. (8.32) will be discussed later.

8.1.6 Application of the Droplet Growth Equation

Simulation of an air parcel ascent is best conducted with a Lagrangian parcel model, which moves with the air parcel. It can simulate the evolution of droplet sizes, droplet number concentrations, and saturation ratio as a function of height above cloud base. A Lagrangian parcel model can be initialized with a population of aerosol particles of different sizes, as shown in Figures 8.5 and 8.6. The parcel model used for these simulations numerically solves the droplet radius growth eq. (8.30) (Neubauer, 2009). It is suitable for simulating the microphysical properties of the early stages of cloud formation, where diffusion and condensational growth dominate.

In the example shown in Figure 8.5, the aerosol particles start from a monomodal lognormal distribution of ammonium sulfate particles with $N_a = 1000\,\mathrm{cm}^{-3}$, $\mu_g = 75\,\mathrm{nm}$, and $\sigma_g = 1.5$, as indicated in terms of dry radii in Figure 8.5b. Before they reach cloud base

https://doi.org/10.1017/9781009485654.009 Published online by Cambridge University Press

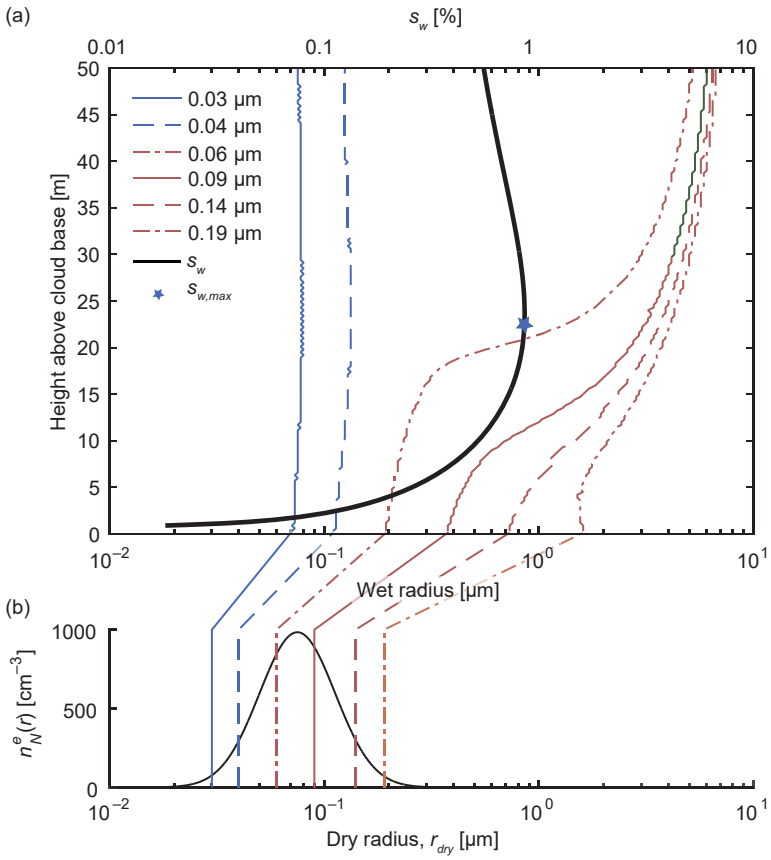


Figure 8.5 (a) Simulated growth of a droplet population as a function of height above cloud base in a rising air parcel without entrainment and with a constant updraft speed of 3 m s^{-1} (Neubauer, 2009). Droplet size (thin lines) corresponds to the lower x-axis and environmental saturation ratio (thick solid line) to the upper x-axis. The initial dry particle size distribution is a monomodal log-normal distribution for ammonium sulfate particles with $N_a = 1000\,\text{cm}^{-3}$, as indicated by the solid curve in panel (b). Data courtesy of David Neubauer.

in Figure 8.5a, the ammonium sulfate particles have deliquesced and grown hygroscopically (Section 7.3). This explains the size shift between panels 8.5b and 8.5a.

The supersaturation reaches its peak at 20–25 m above cloud base in Figure 8.6, marked by the red crosses in the supersaturation profiles. Up to this altitude, all particles are growing and thereby reduce the environmental water vapor. After the peak supersaturation $s_{w,max}$ has been surpassed, the droplet population diverges. The non-activated aqueous solution droplets with dry radii of 0.03–0.04 µm shrink (blue lines), according to Köhler theory (Figure 7.13), in order to remain in equilibrium with the decreasing environmental supersaturation, while the aqueous solution droplets that have been activated into cloud droplets (red lines) continue

https://doi.org/10.1017/9781009485654.009 Published online by Cambridge University Press

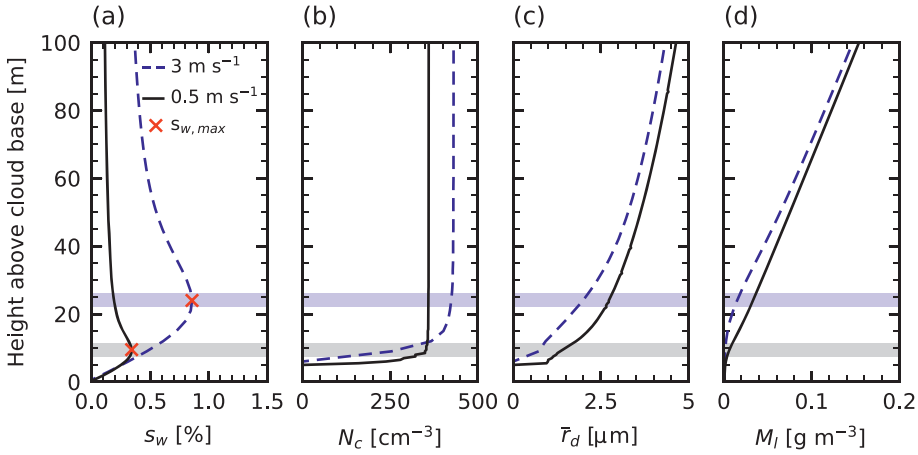


Figure 8.6 Simulated development of cloud properties in the lowest 100 m of a cloud for air ascending at constant updraft speeds of 0.5 $m\,s^{-1}$ and 3 $m\,s^{-1}$ starting at 850 hPa and 15 °C with the same initial aerosol size distribution as in Figure 8.5. (a) Supersaturation s_w, (b) cloud droplet number concentration N_c, (c) mean volume radius $\bar{r}_d$, and (d) liquid water content M_l. Horizontal gray and blue bands mark heights at which the maximum supersaturations $s_{w,max}$ are reached for the different updraft speeds. Data courtesy of David Neubauer.

to grow by condensation. The separation in size between activated cloud droplets and non-activated solution droplets in Figure 8.5 depends on the peak supersaturation, which again is governed by Köhler theory. According to eq. (8.32), the peak supersaturation is determined by the updraft speed: a higher updraft speed activates more aerosol particles. In addition to its dependence on the updraft speed, the number of cloud droplets formed depends on the aerosol size, number concentration, and chemical composition (e.g., Kirschler et al., 2022). The cloud droplets experience rapid growth even at decreasing saturation ratios, because of their size-dependent equilibrium saturation ratio (eq. 7.30), which decreases with increasing droplet size. As the droplets continue to grow, their spread in size becomes narrower because of the parabolic form of the droplet radius growth equation (eq. 8.31) as shown in Figure 8.4.

The dependence of some key cloud properties on the height above cloud base for the early stages of cloud formation is shown in Figure 8.6 for the lowest 100 m in a cloud for two different updraft speeds, 0.5 and 3 $m\,s^{-1}$. As in Figure 8.5, supersaturation first sharply rises and then gently settles when going upward from the cloud base (Figure 8.6a). The peak supersaturation is reached within the first 30 m above cloud base in these examples. The supersaturation approaches a constant value higher up in the cloud when the rate of condensation approaches the production of supersaturation in the updraft. Within the 100 m above cloud base shown in Figure 8.6, Q_1 (eq. 8.33) and Q_2 (eq. 8.34) can be regarded as constant because T, ρ_a, and $e_{s,w}$ vary only a little over this small height range. A constant w implies that the source of supersaturation is approximately constant (eq. 8.32). In fact, the shape of the supersaturation profile in Figure 8.6a is determined by the profile of the condensation rate. The condensation rate is low initially when only a few aqueous solution droplets are activated and increases steadily with the increasing number of activated aqueous solution droplets and thus the larger surface area

https://doi.org/10.1017/9781009485654.009 Published online by Cambridge University Press

that becomes available for condensation. Once the condensation rate exceeds the production rate, it reduces the supersaturation and therefore decreases because of the lowered water vapor gradient between the environmental air and the droplets.

The total cloud droplet number concentration N_c initially increases rapidly but then settles to a constant value at the height where $s_{w,max}$ is reached (Figure 8.6b). The reason is that $s_{w,max}$ determines the number (and thus indirectly the subsequent size) of the activated aerosol particles. Thus, the cloud droplet number concentration is determined in the lowest layers of a cloud. It is smaller for a slower updraft speed because a smaller updraft speed leads to a lower production of supersaturation and thus to a smaller $s_{w,max}$, causing fewer droplets to become activated.

Both the volume mean droplet radius $\bar{r}_d$ (Figure 8.6c) and the liquid water content M_l (Figure 8.6d) increase with the height above cloud base. When fewer droplets compete for the available water vapor, the droplets are on average larger in these clouds. In the first 100 m, mixing with the environment through entrainment and detrainment is negligible and M_l equals approximately its adiabatic value, that is, air density times the adiabatic liquid water content ($M_l \approx \rho_a w_l$; eq. 3.115). w_l, the adiabatic liquid water mixing ratio (Section 3.5.10), increases almost linearly with height in shallow clouds (Brenguier et al., 2000). Clouds for which this so-called *adiabatic assumption* is justified are, for example, stratocumulus clouds with a vertical extent smaller than 1 km (Table 1.3). In the example of Figure 8.6, the factor of three increase in $s_{w,max}$ causes N_c to increase by roughly 25%. The condensation rate, which depletes the supersaturation (eq. 8.32), is linearly proportional to N_c. Therefore, it also only increases by 25%, that is, much less than the production rate of supersaturation. On the whole, the supersaturation remains larger for larger updraft speeds, and less water is found in the condensed phase in the lowest 100 m of the cloud, that is, M_l is slightly smaller at a given altitude.

8.2 Droplet Growth by Collision–Coalescence

Higher up in the cloud, higher than what is shown in Figure 8.6, other processes become important, such as the entrainment of environmental air and the formation of precipitation-sized hydrometeors by collision–coalescence. The main challenge of microphysics in warm clouds is to explain how raindrops can be formed in 20–30 min (Saunders, 1965; Stephens and Haynes, 2007), the typical time period between the first appearance of a cumulus cloud and the earliest appearance of rain drops (Stephens and Haynes, 2007). Because of the decreasing condensational growth rate for increasing cloud droplet radius, condensational growth is usually too slow to be responsible for the observed time scale of rain formation, so other microphysical mechanisms are needed to explain the initiation of rain in warm clouds (Beard and Ochs, 1993).

In fact, *growth by collision–coalescence* is the dominant precipitation formation process in warm clouds. It refers to the collision of droplets of the same or different sizes that then merge together (coalescence) to form a larger drop. Collision–coalescence starts once some droplets exceed a radius of about 15 μm, an empirically determined threshold. Different thresholds varying between 14 μm (Rosenfeld and Gutman, 1994; Rosenfeld et al., 2012) and 20 μm (Wallace and Hobbs, 2006) have been reported. At larger droplet sizes, the droplets can achieve a

https://doi.org/10.1017/9781009485654.009 Published online by Cambridge University Press

100-fold increase in radius (from 5 μm cloud droplets with a number concentration of $10^2\,\mathrm{cm}^{-3}$ to 0.5 mm raindrops with a number concentration of $10^{-4}\,\mathrm{cm}^{-3}$ (Figure 8.1) by collision–coalescence. The collision–coalescence process is rather efficient, given that a raindrop of 0.5 mm radius results from around 10^5 collisions (Rogers and Yau, 1989).

As shown in Figure 8.4, cloud droplets can grow by condensation to $r = 15$ μm in less than 5 min at high temperatures if $s_w \geq 0.5\,\%$. Droplets with sizes larger than about 15 μm begin to settle (Section 8.2.2). The sedimentation of droplets is important because it causes them to collide with smaller droplets in their paths, similar to the wet-scavenging processes discussed for aerosol particles in Section 6.4.1. In clouds with a variety of different cloud droplet sizes, some of which have radii larger than ~15 μm, growth by collision–coalescence becomes the dominant precipitation-formation process. Cloud droplets of different sizes are needed to overcome the *colloidal stability* of the cloud, and hence to initiate growth by collision–coalescence and ultimately to form drizzle and rain in warm clouds (Squires, 1958).

This variety of droplet sizes cannot be caused by condensational droplet growth alone, because it leads to a narrowing of the droplet size spectrum instead of a broadening (Figure 8.5). A broadening of the cloud droplet size distribution, with an associated increase in the sedimentation velocity difference between the largest and smallest droplets, is needed for the onset of precipitation formation as discussed later.

As shown schematically in Figure 8.7, the condensational growth of droplets tends to level off at larger droplet sizes owing to the parabolic form of eq. (8.31). At larger droplet sizes, growth by collision–coalescence takes over. In between, there is a so-called *growth gap* or *growth bottleneck* (Grabowski and Wang, 2013; Lamb and Verlinde, 2011). Possibilities of how this growth gap can be overcome include the presence of giant cloud condensation nuclei (GCCN) (giant aerosol particles, Table 6.1), turbulence, or by considering growth by collision–coalescence as a stochastic process (Section 8.2.4). We will discuss these possibilities later, after introducing the basic concepts needed to understand the collision–coalescence process.

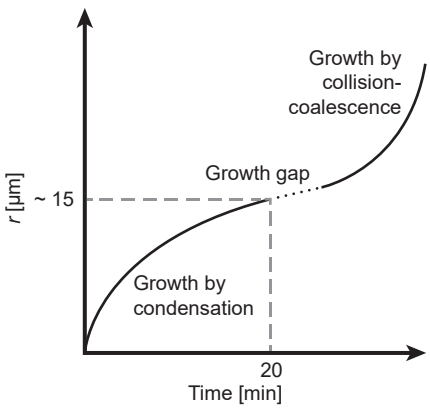


Figure 8.7 Schematic illustration of the growth in droplet radius versus time due to condensation from the vapor phase (eq. 8.31) and by collision–coalescence beyond the growth gap.

https://doi.org/10.1017/9781009485654.009 Published online by Cambridge University Press

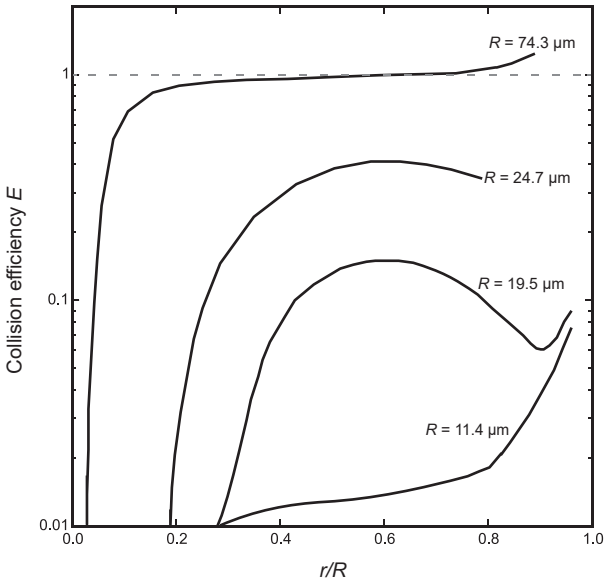


Figure 8.8 Computed collision efficiencies E for pairs of drops as a function of the ratio of their radii, r/R for a constant R. The curves are labeled according to the radius R of the larger collector drop. Figure adapted from Schlamp et al. (1976). ©American Meteorological Society. Used with permission.

8.2.1 Collision and Coalescence Efficiencies

Collisions may occur due to gravitational settling once some drops become larger than others. The probability of collisions is expressed in terms of the collision efficiency E (eq. 6.19). Collision efficiencies from theoretical calculations for collector drops with radii R between 11 and 74 μm and smaller droplets of radius r are shown in Figure 8.8 as a function of the ratio of their radii, r/R (Schlamp et al., 1976). The collision efficiency E is small for small values of r/R. Here, the collected droplets are small, have little inertia, and are thus easily deflected by the air flow around the collector drop (Figure 6.8). The inertia increases with increasing mass of the small droplets and thus with increasing values of r/R. The value of E increases up to approximately $r/R = 0.6$. Beyond this ratio, two counteracting effects influence E. On the one hand, the difference in size between the collector drop and the collected droplet becomes smaller. As the inertia of the smaller (collected) droplet increases, it is less likely to be deflected around the collector drop. On the other hand, the forces of deflection have a longer time to operate, because the velocity of the two droplets is more similar, leading to a decrease in E.

There is also the possibility that a trailing drop will be attracted into the wake of a drop falling close by at a similar speed (Woods and Mason, 1965; Hu et al., 1998; Ren et al., 2020). This can cause a capture from behind, which is called *wake capture*. For a given r/R ratio, wake capture is more important for larger collector drops (Figure 6.8) because they induce more turbulence, which pulls the trailing drops into their wake. Wake capture can be compared to cycling in the lee of another bicycle. Cycling with the same power in the lee of someone would cause a collision because the person cycling in front experiences the full aerodynamic resistance, whereas the person behind experiences a much reduced aerodynamic resistance. Likewise, the lower drop experiences the full aerodynamic resistance as it falls gravitationally, whereas the drop falling in its wake experiences a much reduced aerodynamic resistance,

https://doi.org/10.1017/9781009485654.009 Published online by Cambridge University Press

causing it to fall at a higher velocity, which might induce a collision with the drop below. Because the expression of E in eq. (6.19) does not take wake capture into account, the calculated E can slope upward at large ratios of r/R and exceed 100 % for large collector drops (Figure 8.8).

So far, we have assumed that colliding drops stick together, that is, coalesce. This, however, is only one of three possibilities. If two drops collide, the following can happen: (i) they coalesce and remain permanently united, (ii) they coalesce temporarily and then break into a number of smaller drops, or (iii) they coalesce temporarily and then separate, retaining their initial identities.

If both drops have radii below 100 μm, (i) is the most important process, corresponding to regime I in Figure 8.9. The coalescence efficiency $\hat{E}$ is defined as the number of coalescence events divided by the total number of collisions. The growth of droplets by collision–coalescence is governed by the collection efficiency $\tilde{E}$, which is the product of the coalescence efficiency and the collision efficiency:

$$\tilde{E} = \hat{E} \cdot E. \tag{8.35}$$

A good assumption for the collision–coalescence process for droplets and drops with $r < 100\,\mu\text{m}$ is that $\hat{E} \sim 1$, so that $\tilde{E} = E$. Case (ii) is important if two raindrops ($r > 100\,\mu\text{m}$) collide (Beard and Ochs, 1995) and break-up occurs, corresponding to regime II in Figure 8.9. Break-up will be further discussed in Section 8.3. A temporary coalescence or rebound collision as in case (iii) occurs rather seldomly in the atmosphere (Testik, 2009; Testik et al., 2011) (regime III in Figure 8.9), but is important for thunderstorm electrification (Section 11.4.4).

8.2.2 Terminal Velocity of Cloud Droplets and Raindrops

To derive the droplet growth equation due to collision–coalescence, we need to know at which speed the droplets fall. A droplet reaches its steady-state sedimentation velocity when the gravitational force is balanced by the drag force. The drag force denotes the aerodynamic resistance exerted on the droplet by the air as a viscous medium, as shown in Figure 8.10. This steady-state sedimentation velocity is called *terminal velocity* v_T to emphasize that a given droplet does not accelerate beyond v_T.

The gravity force F_G on a spherical water droplet with radius r is directed toward Earth's surface (negative z-direction) and is given by the weight of the droplet times the acceleration due to gravity:

$$F_G = m_l g = \frac{4}{3}\pi r^3 g \rho_l, \tag{8.36}$$

The drag force F_D exerted on this droplet in a viscous fluid is proportional to its cross-sectional area and is directed in the opposite direction, that is, the positive z-direction and is given by:

$$F_D = \frac{\pi}{2} r^2 v^2 \rho_a C_D = 6\pi\mu r v \left(\frac{C_D Re}{24}\right), \tag{8.37}$$

https://doi.org/10.1017/9781009485654.009 Published online by Cambridge University Press

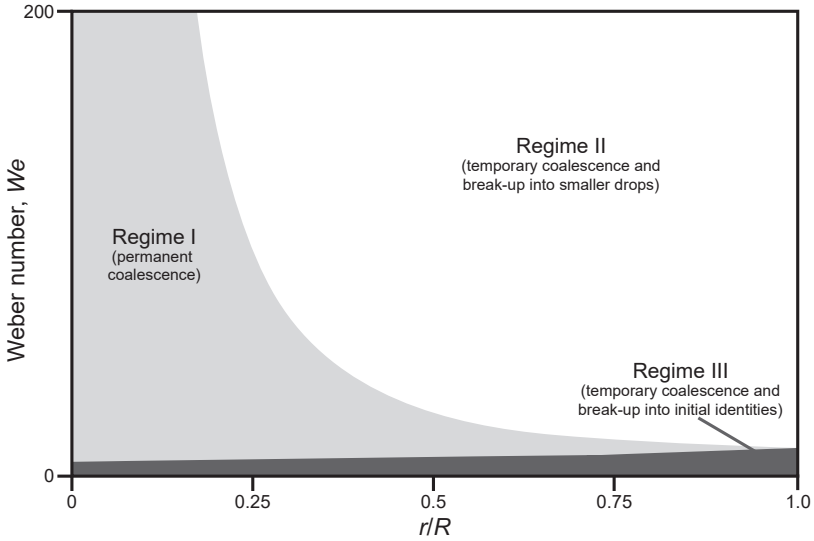
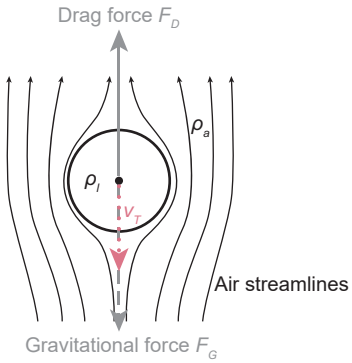


Figure 8.9 Schematic of the outcomes of drop collisions as a function of the Weber number (y-axis) vs. the ratio of the small droplet to the large drop. Regime I is dominated by coalescence, regime II by break-up, and regime III by rebound collisions. The Weber number is defined as the ratio of the collisional kinetic energy (eq. 8.66) divided by the product of v_r (eq. 8.67) times the surface tension of water in air. Figure adapted from Testik (2009).

Figure 8.10 Schematic showing the terminal velocity v_T, defined as the velocity when a balance between the drag force F_D and the gravitational force F_G has been established.



where μ is the dynamic viscosity of air and C_D is the drag coefficient, an empirical factor accounting for all non-geometrical components of the drag force. The Reynolds[3] number Re is a measure of the degree of turbulence. Re is defined as the ratio of the inertial force (Section 4.1) to the viscous force, that is, the friction that attempts to resist the motion of a fluid, as follows:

$$Re = \frac{\vec{u}\nabla\vec{u}}{\nu\nabla^2\vec{u}}. \tag{8.38}$$

[3] www.britannica.com/biography/Osborne-Reynolds

https://doi.org/10.1017/9781009485654.009 Published online by Cambridge University Press

Table 8.2 Typical values for Reynolds numbers *Re* for different liquid hydrometeors at $T_0 = 273.15$ K and $p = 900$ hPa together with some drag coefficients C_D.

Hydrometeor	Radius	*Re*	C_D	Note/Reference
Cloud droplet	$r = 5\,\mu$m	0.01	2400	Assuming $C_D Re/24 \approx 1$, Böhm (1992)
Cloud droplet	$r = 14.4\,\mu$m	0.05	480	Assuming $C_D Re/24 \approx 1$, Böhm (1992)
Drizzle drop	$r = 31.7\,\mu$m	0.5		Böhm (1992)
Drizzle drop	$r = 76.0\,\mu$m	5		Böhm (1992)
Spherical raindrop		10	4.2	Pruppacher and Klett (1997)
Spherical raindrop		100	1.08	Pruppacher and Klett (1997)
Spherical raindrop	> 0.5 mm	> 300	0.45	Rogers and Yau (1989); Lamb and Verlinde (2011)
Raindrop as disk		> 1000	1.17	Hoerner (1965)

Here, ν is the kinematic viscosity. Using scale analysis with the scales typical for a falling raindrop (where length scale = drop diameter and velocity scale = terminal velocity, see Table 1.2), we obtain:

$$Re \sim \frac{v_T^2}{2r}\frac{(2r)^2}{\nu v_T} = \frac{2v_T r}{\nu} = \frac{2\rho_a v_T r}{\mu}. \tag{8.39}$$

Assuming equilibrium between F_D and F_G, the sedimentation velocity that enters the equation for the drag force is the terminal velocity v_T. It can be calculated from

$$6\pi\mu r v_T \left(\frac{C_D Re}{24}\right) = \frac{4}{3}\pi r^3 g\rho_l. \tag{8.40}$$

Rearranging the factors yields the general form of v_T for spherical particles:

$$v_T = \frac{2}{9}\frac{r^2 g\rho_l}{\mu C_D Re/24}. \tag{8.41}$$

Since *Re* and C_D both depend on v_T, eq. (8.40) cannot be solved analytically for v_T. The calculation of v_T depends on a calculation of both *Re* and C_D. However, both *Re* and C_D vary with the type of flow and the drop size (Beard and Pruppacher, 1969; Wang, 2013), making it impossible to give a general expression that is valid for all drop sizes. Examples of typical Reynolds numbers and drag coefficients for liquid hydrometeors are summarized in Table 8.2.

To reduce complexity, we can divide the range of possible drop sizes into different regimes. This allows us to define empirical expressions for the terminal velocities in each individual size regime, when assuming representative values of *Re* and C_D for each regime and hydrometeor type (Figure 8.11 and Table 8.2).

For droplets with radii $r < 40\,\mu$m (cloud droplets and small drizzle drops; Figure 8.1 and Table 1.2), for which $Re \ll 1$ (Table 8.2), the factor $C_D Re/24$ is approximately 1 (Rogers and Yau, 1989) (Figure 8.11). In this case, eq. (8.41) can be simplified to:

$$v_T = \frac{2}{9}\frac{r^2 g\rho_l}{\mu} = k_1 r^2, \qquad r < 0.04\,\text{mm}. \tag{8.42}$$

https://doi.org/10.1017/9781009485654.009 Published online by Cambridge University Press

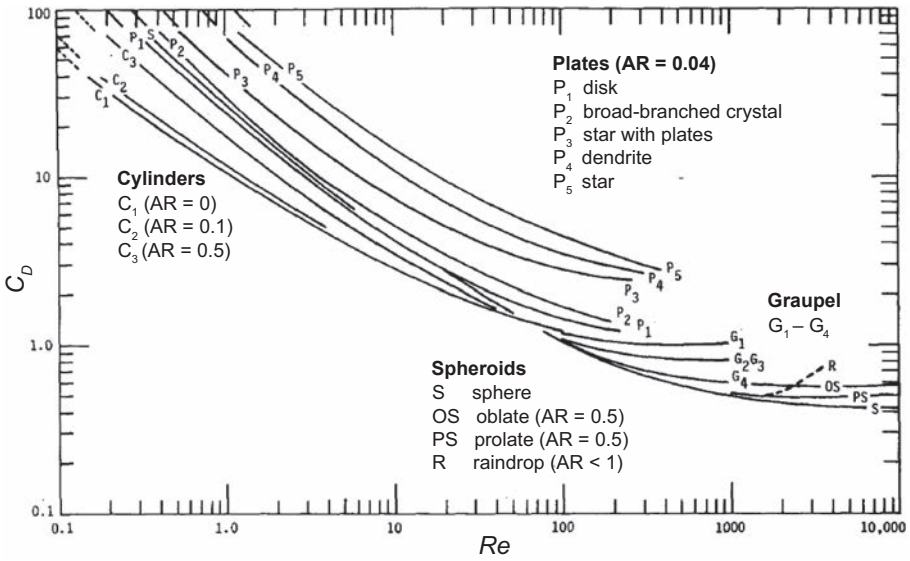


Figure 8.11 Relation between drag coefficient C_D and Reynolds number Re for the flow past different types of liquid or solid hydrometeors, as indicated by the legend. Figure adapted from Beard (1980). ©American Meteorological Society. Used with permission.

This regime is known as the *Stokes*[4] *regime* and eq. (8.42) is known as *Stokes's law* (Stokes, 1851). It is characterized by the quadratic dependence of v_T on drop size. Using the values of $\mu = 1.82 \times 10^{-5}\,\mathrm{kg\,m^{-1}\,s^{-1}}$ at 293.15 K (Table 8.1) and $\rho_l = 998.16\,\mathrm{kg\,m^{-3}}$ at 293.15 K (eq. A.1), we can approximate k_1 as $1.2\times10^{6}\,\mathrm{cm^{-1}\,s^{-1}}$. Using this k_1 value in eq. (8.42) together with r in units of cm, yields v_T in $\mathrm{cm\,s^{-1}}$.

For hydrometeors with radius in the range $40\,\mu\mathrm{m} < r < 0.6\,\mathrm{mm}$, an empirical formula for their terminal velocity is given by Rogers and Yau (1989) as

$$v_T = k_2 r, \qquad 0.04\,\mathrm{mm} < r < 0.6\,\mathrm{mm}, \tag{8.43}$$

with $k_2 = 8000\,\mathrm{s^{-1}}$, v_T in $\mathrm{cm\,s^{-1}}$, and r in cm. Thus, in this regime, v_T varies approximately linearly with the hydrometeor radius.

For raindrops with $r > 0.6\,\mathrm{mm}$, for which $Re > 300$, C_D is less dependent on Re (Figure 8.11). Assuming a value of $C_D = 0.45$ (Rogers and Yau, 1989), eq. (8.41) becomes

$$v_T = \frac{2}{9}\frac{24r^2 g\rho_l}{0.45\mu Re} = \frac{2}{9}\frac{24r^2 g\rho_l \mu}{0.45\mu 2\rho_a v_T r}. \tag{8.44}$$

Here, the Reynolds number has been replaced by its definition (8.39). Rearranging factors yields

$$v_T^2 = \frac{rg\rho_l}{\rho_a}\frac{160}{27}, \tag{8.45}$$

[4] www.britannica.com/biography/Sir-George-Gabriel-Stokes-1st-Baronet

https://doi.org/10.1017/9781009485654.009 Published online by Cambridge University Press

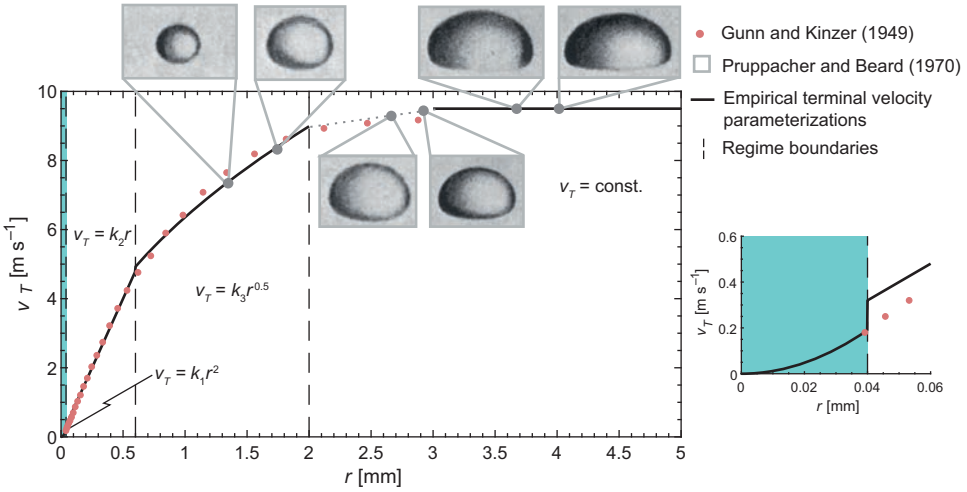


Figure 8.12 Terminal velocities of cloud droplets, drizzle drops, and raindrops up to 2 mm radius using eqs. (8.42), (8.46), and (8.43). The vertical dashed lines mark the separations between the different terminal velocity regimes. The v_T of drops between 2 and 3 mm is shown qualitatively to indicate the transition to a constant terminal velocity for raindrops larger than 3 mm. The inset photographs are of raindrops with equivalent radii of 1.35 mm, 1.73 mm, 2.65 mm, 2.9 mm, 3.7 mm, and 4 mm. Also shown are measured terminal droplet velocities from Gunn and Kinzer (1949). These measurements were done in stagnant air for $p = 1013$ hPa, $T = 293$ K, and $\mathrm{RH}_w = 50\,\%$. The graph on the right-hand side shows a zoom to the region $r < 0.05$ mm, where v_T is given by $v_T = k_1 r^2$. Photographs taken from Pruppacher and Beard (1970) with permission from Wiley.

or

$$v_T = k_3 \sqrt{r}, \qquad 0.6\,\mathrm{mm} < r < 2\,\mathrm{mm}, \tag{8.46}$$

with $k_3 \approx 2.01 \times 10^3\,\mathrm{cm}^{1/2}\,\mathrm{s}^{-1}$ for a raindrop radius in cm between 0.6 and 2 mm and v_T in $\mathrm{cm\,s}^{-1}$ (Rogers and Yau, 1989). The upper limit corresponds to the size up to which raindrops can be considered spherical.

Figure 8.12 summarizes the terminal velocity as a function of droplet size, where the dashed lines mark the separations between the different regimes. Because of their empirical character, the transitions between the different formulas are not smooth.

Figure 8.12 also illustrates how falling raindrops in air become increasingly non-spherical with increasing size, as indicated by the insets (Pruppacher and Beard, 1970). The bottom of the raindrops flattens considerably beyond a raindrop radius of 2 mm (Pruppacher and Pitter, 1971; Beard and Chuang, 1987; Szakáll et al., 2010). Such changes in raindrop shape need to be considered when determining their terminal fall velocities (Loftus and Wordsworth, 2021). Related to this, the raindrop sizes in Figure 8.12 are given in terms of the equivalent spherical radius, that is, the radius which one would obtain if a raindrop of that given mass was spherical. A raindrop with an equivalent size of 2.5 mm can be considered as an oblate spheroid (Figure 8.12). Because of its large cross-sectional area, its drag force approaches the same

https://doi.org/10.1017/9781009485654.009 Published online by Cambridge University Press

radius dependence as the gravitational force acting on the drop. Its terminal velocity is thus approximately constant for equivalent raindrop radii $>$ 2.5 mm. The maximum equivalent raindrop radius is limited by break-up (Section 8.3). Depending on the environmental pressure and temperature, the maximum equivalent raindrop radius varies between 3 and 5 mm (e.g., Hobbs and Rangno, 2004; Gatlin et al., 2015; Loftus and Wordsworth, 2021).

8.2.3 Growth Model for Continuous Collection

For drops to collide, they generally have to have different velocities and thus different sizes (in the absence of turbulence and wake capture). Consider a raindrop (collector drop) with radius R falling with terminal velocity $v_T(R)$ through a population of smaller droplets of uniform sizes r, falling at terminal velocities $v_T(r)$. During settling, the collector drop can collide with smaller droplets in its path if they are located within the impact parameter x_0 of the collector drop (eq. 6.19 and Figure 6.8). As in the case of the wet scavenging of aerosol particles discussed in Section 6.4.1, we can define the cross-sectional area as $\pi(R+r)^2$. Hence, the volume swept out by the collectordrop per unit time is given as:

$$\frac{dV_{sweep}}{dt} = \pi(R+r)^2[v_T(R) - v_T(r)]. \tag{8.47}$$

Furthermore, we can express the mass growth rate of the collector drop as the product of the rate of change of sweep-out volume V_{sweep} times the collection efficiency $\tilde{E}(R,r)$ and the cloud liquid water content M_l in kg m^{-3} of the smaller droplets:

$$\frac{dm_R}{dt} = \frac{dV_{sweep}}{dt}\tilde{E}(R,r)M_l = K(R,r)M_l, \tag{8.48}$$

where $K(R,r)$ (m^3 s^{-1}) is the gravitational collection kernel:

$$K(R,r) = \pi(R+r)^2[v_T(R) - v_T(r)]\tilde{E}(R,r). \tag{8.49}$$

M_l is given as

$$M_l = \int_0^R \frac{4}{3}\pi\rho_l r^3 n_N(r)dr. \tag{8.50}$$

Here, $n_N(r)$ is the number size distribution function, denoting the number of cloud droplets of radius r per unit volume of air. It can be treated in an identical fashion as discussed for aerosol particles (eq. 6.1). For the derivation so far, we have assumed that the cloud consists of a continuum of droplets of uniform size that are homogeneously distributed in space. We can apply eq. (8.48) to a collector drop falling through a more realistic polydisperse cloud droplet population, where each droplet of radius r_i has its own liquid water content $M_{l,i}$ and collection efficiency $\tilde{E}(R,r_i)$. Treating the cloud droplet population as a continuum, we can generalize eq. (8.48) by integrating over the size range where collection by the collector drop with radius R can occur. The mass growth rate of the collector drop can then be written as:

$$\frac{dm_R}{dt} = \frac{dV_{sweep}}{dt}\tilde{E}(R,r)M_l = \int_0^R \pi(R+r)^2[v_T(R) - v_T(r)]\tilde{E}(R,r)\frac{4}{3}\pi\rho_l r^3 n_N(r)dr. \tag{8.51}$$

https://doi.org/10.1017/9781009485654.009 Published online by Cambridge University Press

To express the growth rate in terms of the change in radius of the large collector drop R in time, we replace dm_R with $4\pi\rho_l R^2 dR$ in eq. (8.51) and rearrange the equation to:

$$\frac{dR}{dt} = \frac{\pi}{3}\int_0^R \left(\frac{R+r}{R}\right)^2 [v_T(R) - v_T(r)] n_N(r) r^3 \tilde{E}(R,r) dr. \tag{8.52}$$

If the collected droplets are much smaller than the collector drop, $R + r$ can be approximated as R and the terminal velocity $v_t(r)$ can be neglected, so that $v_T(R)$ can be moved in front of the integral:

$$\frac{dR}{dt} \approx \frac{\pi}{3} v_T(R) \int_0^R n_N(r) r^3 \tilde{E}(R,r) dr. \tag{8.53}$$

To integrate this equation, we assume an average collection efficiency for the droplet population, $\bar{\tilde{E}}$. This simplification is justified when the size distribution of the cloud droplets is narrow, leading to

$$\frac{dR}{dt} \approx \frac{\pi}{3} \bar{\tilde{E}} v_T(R) \int_0^R n_N(r) r^3 dr. \tag{8.54}$$

From eq. (8.54), we see that the radius growth rate for growth by collection per unit time is proportional to the size of the small droplets cubed (r^3). Substituting eq. (8.50) in eq. (8.54), we obtain the continuous radius growth rate of the collector drop as:

$$\frac{dR}{dt} \approx \frac{\bar{\tilde{E}} M_l v_T(R)}{4\rho_l} = \alpha v_T(R). \tag{8.55}$$

We can integrate this equation for the different growth regimes and obtain for collector drops in the Stokes regime ($R < 40\,\mu m$):

$$R(t) = \frac{R_0}{1 - \alpha t R_0}, \tag{8.56}$$

showing the initial linear radius growth due to collision–coalescence (Figure 8.7). In the linear fall velocity regime ($40\,\mu m < R < 600\,\mu m$), we obtain:

$$R(t) = R_0 \exp(\alpha k_2 t), \tag{8.57}$$

which shows the exponential growth with time, due to collision–coalescence for collector drops $> 40\,\mu m$ (Figure 8.7). By contrast, the radius growth for diffusional growth only increases proportional to $\sqrt{t}$. This explains the fundamental difference between these two growth mechanisms (Figure 8.13) and why growth by collision–coalescence is needed to explain the formation of rain in warm clouds that is often observed within 20–30 min of cloud formation (Saunders, 1965; Stephens and Haynes, 2007).

Looking back at eq. (8.52), we can deduce that the growth rate of the collector drop is extremely sensitive to the droplet droplet size distribution $n_N(r)$: The broader the distribution, the faster the growth because the relative velocities between the drops are larger. Growth by collision–coalescence is an accelerating process, since the terminal velocity of the collector drop $v_T(R)$ increases with increasing R and the growth rate dR/dt also increases with increasing R.

https://doi.org/10.1017/9781009485654.009 Published online by Cambridge University Press

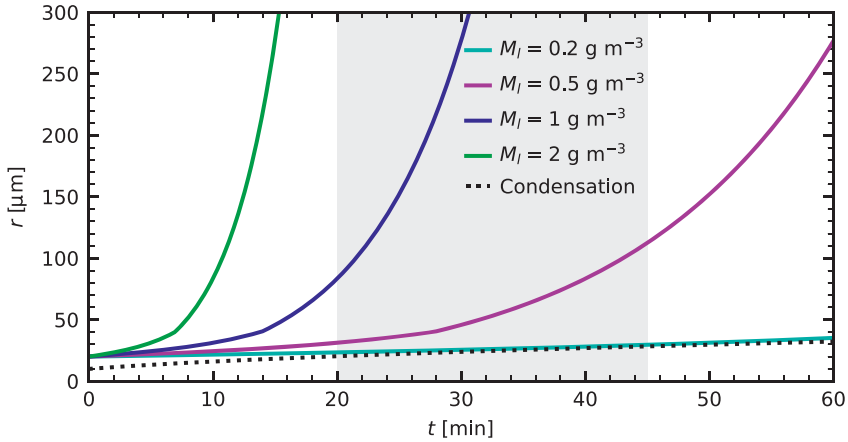


Figure 8.13 Calculated growth times for growth by condensation (line, eq. 8.31 starting from spherical droplet with a radius of 10 µm) versus growth by collision–coalescence (eq. 8.55 starting from a 20 µm droplet) for conditions that are typical of a cumulus cloud ($T = 273.15$ K, $p = 800$ hPa, $S_w = 1.002$, $\bar{\bar{E}} = 1$ and four different values of M_l: 0.2, 0.5, 1 and 2 g m^{-3}; colored lines). The typical lifetime for a cumulus congestus cloud of 20–45 min (Table 1.3) is indicated by the gray shaded region.

This is in strong contrast with growth by condensation, where the increase in radius over time is proportional to $t^{1/2}$ (eq. 8.31 and Figure 8.7). Nevertheless, diffusional growth still takes place. In fact, it provides the small droplets that feed the growth of the large collector drop by collision–coalescence. As the collision efficiency E also increases with increasing size of the small droplets (Figure 8.8), diffusional growth actually helps to speed up the growth by collision–coalescence.

Equation (8.55) describes droplet growth as a continuous collection process. However, in reality, growth by collision–coalescence is not purely continuous but occurs stepwise by random collisions. In a probabilistic sense, these collisions are very rare for small droplet sizes and increasingly likely for larger droplet sizes. Approximating droplet growth as a continuous collection process cannot capture the non-linear increase in collision efficiency for increasing r/R ratio as shown in Figure 8.8. Moreover, the continuous collection model predicts time scales for warm rain formation, or more precisely the formation of precipitation sized drops, which can be larger than those typically observed (Jonas, 1996).

Figure 8.13 shows a comparison of growth by condensation with $s_w = 0.2\,\%$ versus growth by continuous collision-coalescence in still air (in the absence of turbulence) for typical cumulus cloud conditions of M_l ranging between 0.2 and 2 g m^{-3} (Table 1.3), assuming $\bar{\bar{E}} = 1$. It illustrates that it takes the droplet 20 min to grow from 10 µm to 20 µm by condensation. For $M_l = 1$ g m^{-3} or less, it takes at least 30 min to grow from 20 µm to 300 µm by collision–coalescence. In this case, the combined growth time is 50 min, which is longer than the typical lifetime of the smallest precipitating cumuli, which typically ranges from 20 to 45 min (Cu con, Table 1.3). However, if $M_l = 2$ g m^{-3}, which is close to the observed upper LWC value for Cu

https://doi.org/10.1017/9781009485654.009 Published online by Cambridge University Press

con (Table 1.3), then growth by continuous collision–coalescence only takes half as long, so that the combined condensational and collisional growth allows to achieve precipitation-sized drops within the cloud's lifetime.

8.2.4 Growth Model for Stochastic Collection

A more realistic approach to the collection process by collision–coalescence is found by describing it stochastically. This accounts for the randomness of the distribution of cloud droplets that makes a prediction of the exact location and timing of a collision process impossible. The stochastic collection equation (SCE) expresses the stochastic growth of cloud droplets in terms of the probability that a larger drop will collect another droplet of any smaller size. It also takes into account the probability for every possible combination of drops to collide and coalesce and how these probabilities change after each collection event (Berry, 1967). In this stochastic approach, the collision efficiency is the probability that a drop of radius R collects a droplet of radius r located at a random position in its sweep-out volume. The SCE can be written in terms of the temporal evolution of the droplet mass size distribution function $f(m_x, t)$, where m_x is the drop mass and t is the time:

$$\frac{\partial f(m_x,t)}{\partial t} = \frac{1}{2}\int_0^{m_x} f(m_x - m_y, t) f(m_y, t) K(m_x - m_y, m_y) dm_y - \int_0^{\infty} f(m_x, t) f(m_y, t) K(m_x, m_y) dm_y. \tag{8.58}$$

Here, $m_x - m_y$ and m_y refer to the pair of drops colliding in the collision–coalescence process with collection kernel $K(m_x - m_y, m_y)$ (eq. 8.49). In the SCE, droplet mass is used because mass is conserved during the collision–coalescence process, but the number concentration of the hydrometeors decreases (in the absence of break-up). The first term in eq. (8.58) corresponds to a source of drops arriving at mass m_x after collision–coalescence. The second term corresponds to a sink of drops of mass m_x due to collision–coalescence with drops of all other sizes. The factor $1/2$ in the first term avoids the double counting of collection events. Solving the SCE, however, requires knowledge of the collection kernel K.

An example of the stochastic evolution of a droplet mass distribution for which collision–coalescence is the only growth mechanism is shown in Figure 8.14. Here, the droplet growth is calculated using an approach that divides the hydrometeor mass distribution into three size classes (cloud droplets, drizzle drops, and raindrops), describing each class with a modified gamma distribution (eq. 1.1). In Figure 8.14, the growth starts from a hydrometeor population consisting purely of cloud droplets. The cloud droplet mass distribution was initiated with a cloud droplet number concentration $N_c = 75\,\mathrm{cm}^{-3}$ and a liquid water content $M_l = 7.5 \times 10^{-4}\,\mathrm{kg\,m}^{-3}$, corresponding to a mean radius of 13.4 μm. In this clean cloud, drizzle is produced early on, as indicated in Figure 8.14 by the bimodal mass distribution appearing at $t = 5$ min. With ongoing time, the initial narrow distribution becomes broader as cloud droplets collide and form larger hydrometeors. At the same time, the number concentration of the cloud droplets decreases. Raindrops are formed after around 15 min, that is, much faster than when treating collision–coalescence as a continuous process. Although relatively few in number initially, these large drops grow rapidly and dominate the mass distribution.

https://doi.org/10.1017/9781009485654.009 Published online by Cambridge University Press

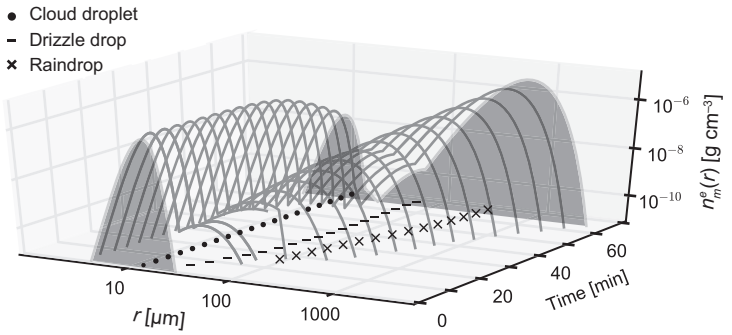


Figure 8.14 Three-dimensional illustration of the temporal evolution of a hydrometeor number size distribution (cloud droplets, drizzle drops, and raindrops) in an idealized simulation over 70 min in steps of 200 s, solving the stochastic collection equation. The cloud droplet population was initialized with a total number concentration $N_c = 75\,\mathrm{cm}^{-3}$ and a cloud water content $M_l = 0.75\,\mathrm{g\,m}^{-3}$ indicated by the gray shaded mass distribution at $t = 0$. Figure adapted from Sant et al. (2013). ©American Meteorological Society. Used with permission.

Once rain is formed, the cloud droplet number concentration decreases noticeably, starting at around 50 min. At the end of the simulation, after 70 min, hardly any cloud droplets remain and the drizzle has been entirely converted to rain. Since this idealized simulation comprises only the collision–coalescence process, the raindrops neither sediment nor evaporate.

8.2.5 Speed-up of Collision-Coalescence Due to Giant Cloud Condensation Nuclei and Turbulence

The drop size distribution can be broadened toward larger droplet radii in the presence of GCCN (Johnson, 1982; Jensen and Lee, 2008; Blyth et al., 2003). These could be, for example, sea salt particles over the oceans or mineral dust, biological particles, or urban aerosols, such as road dust particles (Johnson, 1976; Van Malderen et al., 1992) over the continents.

Figure 8.4 illustrates the effect of GCCN, showing that a droplet grown from a 10 μm aerosol particle remains considerably larger than those grown from smaller particles over the calculated 30 min at $T = 253\,\mathrm{K}$. In fact, the relatively low observed number concentrations of GCCN over the ocean, between 10^{-4} and 10^{-2} cm^{-3} are sufficient to affect drizzle production and transform a non-precipitating stratocumulus into a precipitating state, as shown in a modeling study by Feingold et al. (1999), with implications for cloud microphysical and radiative properties. The impact of GCCN on surface precipitation is further illustrated in Figure 8.15, for different CCN number concentrations and GCCN sizes. It shows results from a global climate model simulation where the GCCN number concentration was varied between 10^{-4} and 1 cm^{-3}, the number concentrations of the background CCN were taken as 100 cm^{-3}, 250 cm^{-3}, and 500 cm^{-3} and the raindrops grown from activated GCCN were assumed to have initial dry sizes of 12 μm, 25 μm, and 55 μm. In the case with the lowest

https://doi.org/10.1017/9781009485654.009 Published online by Cambridge University Press

CCN number concentrations (N_{CCN}), some precipitation is formed through condensational growth and collision–coalescence regardless of the GCCN concentration. These clouds have on average larger cloud droplets and a broader size distribution (Figure 1.23), and the addition of GCCN has less impact for their ability to produce precipitation. On the contrary, the smaller precipitation rate in clouds with higher CCN concentrations is caused by a less efficient collision–coalescence process due to the smaller size of the individual droplets. The impact of GCCN on precipitation is hence smallest for the cleanest cloud, with N_{CCN} = 100 cm^{-3}, and largest for the most polluted cloud, with N_{CCN} = 500 cm^{-3}. Thus, the addition of GCCN typically matters most for continental clouds and is usually negligible for marine clouds, which mostly consist of fewer cloud droplets (Table 1.3 and Figure 1.22). We further note that the sizes of the GCCN are of minor importance compared to their number concentration, especially for clean conditions and for the sizes assumed here (Figure 8.15).

If no GCCN are present, turbulence is needed to explain the broadening of the cloud droplet size distribution. Turbulence, the random fluctuations of air masses superimposed on the mean

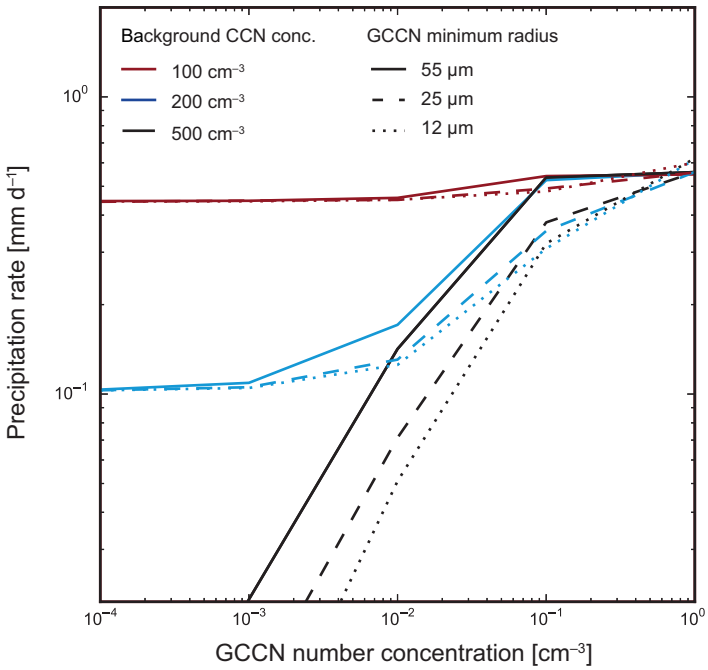


Figure 8.15 Precipitation rate as a function of the GCCN concentration. The (background) CCN number concentrations N_{CCN} are indicated in the plot as follows: top group of lines, $N_{CCN} = 100\,cm^{-3}$; middle group, $N_{CCN} = 250\,cm^{-3}$; bottom group, $N_{CCN} = 500\,cm^{-3}$. For each value of N_{CCN}, three minimum radii of the GCCN, r_{GCCN}, were used: $r_{GCCN} = 55\,\mu m$ (solid lines), $r_{GCCN} = 25\,\mu m$ (dashed lines), and $r_{GCCN} = 12\,\mu m$ (dotted lines). The simulations were conducted with the single-column model version of the ECHAM5-HAM global climate model. Data courtesy of Vivek Sant.

https://doi.org/10.1017/9781009485654.009 Published online by Cambridge University Press

air motion, is always present in clouds to some degree (Shaw, 2003; Siebert et al., 2006). Turbulent fluctuations promote coalescence by increasing the probability of droplet collisions, or by promoting diffusional growth due to turbulent fluctuations in supersaturation (Vaillancourt and Yau, 2000; Falkovich et al., 2002; Grabowski and Wang, 2013). In particular, the presence of turbulence causes droplets to have a relative velocity not only in the vertical direction due to gravitational settling but in all directions due to the random air motions (Vohl et al., 1999; Franklin, 2014; Krueger and Kerstein, 2018). The collision kernel (eq. 8.49), a measure of the collision efficiency, increases due to turbulence by up to a factor of five (Wang and Grabowski, 2009; Grabowski and Wang, 2013).

Yet another mechanism that can speed up or induce collision–coalescence is mixing. For example, entrainment of dry environmental air masses at the cloud–air boundaries can impact the cloud droplet size distribution and induce conditions that favor the hygroscopic growth and activation of GCCN (Small and Chuang, 2008). The different mechanisms that can speed up the collision–coalescence process are not mutually exclusive, but can act simultaneously. For example, it has been observed that GCCN that initiate precipitation formation are preferentially found in the cloud-top regions of cumulus clouds (Small and Chuang, 2008). These cloud top regions are more strongly affected by turbulence generated by entrainment of environmental air (e.g., Desai et al., 2021), which in turn increases the collision rate of the cloud droplets near cloud top (Small and Chuang, 2008).

8.3 Evaporation and Break-up of Raindrops

8.3.1 Evaporation of Cloud Droplets and Raindrops

When the RH_w drops below 100 %, the droplet growth equation can be used to calculate the negative growth, that is, the evaporation rate of cloud droplets and raindrops. Since raindrops are much larger than cloud droplets, the flow around them is more turbulent than around cloud droplets. These turbulent air motions enhance the transport of mass and heat to and away from a droplet, causing the evaporation rate to be larger than that calculated from eq. (8.23).

The turbulent enhancement of the evaporation rate for moving cloud droplets, drizzle, and raindrops is obtained by multiplying the right-hand side of eq. (8.23) by the mean ventilation coefficient $\overline{f}_v$ (Kinzer and Gunn, 1951; Beard and Pruppacher, 1971).

$\overline{f}_v$ is defined as the ratio of the water mass flux to or from a moving drop dm_l/dt to that of a motionless drop $(dm_l/dt)_0$:

$$\overline{f}_v \equiv \frac{dm_l/dt}{(dm_l/dt)_0}. \tag{8.59}$$

The ventilation coefficient for mass transfer from an evaporating droplet can be expressed as:

$$\overline{f}_v = \alpha + \beta Sc^{1/2} Re^{1/3}. \tag{8.60}$$

Here, Sc is the Schmidt number (eq. 6.20), Re is the Reynolds number Re (eq. 8.39), and α and β are constants over the range $2 \leq Re \leq 2000$ (Beard and Pruppacher, 1971). Numerous

https://doi.org/10.1017/9781009485654.009 Published online by Cambridge University Press

authors have obtained empirical expressions for coefficient $\overline{f}_v$ as a function of Re and Sc (e.g., Wedding et al., 1986; Bhalwankar et al., 2004). For example, based on laboratory data of droplets falling at their terminal velocity in air, Beard and Pruppacher (1971) found

$$\overline{f}_v = 1.0 + 1.08\ (Sc^{1/3}\ Re^{1/2})^2, \tag{8.61}$$

for $0 \leq Sc^{1/3}\ Re^{1/2} \leq 1.4$, and

$$\overline{f}_v = 0.78 + 0.308\ Sc^{1/3}\ Re^{1/2}, \tag{8.62}$$

for $1.4 < Sc^{1/3}\ Re^{1/2} \leq 51.4$. In a later study, Pruppacher and Rasmussen (1979) confirmed that eqs. (8.61) and (8.62) hold for droplets and drops of equivalent radii of $0 \leq r_{eq} \leq 60\,\mu m$ and $60 \leq r_{eq} \leq 2500\,\mu m$, respectively.

Figure 8.16a illustrates the expected linear increase of $\overline{f}_v$ as $Sc^{1/3}\ Re^{1/2}$ for $Sc^{1/3}\ Re^{1/2} > 1.4$ ($60 \leq r_{eq} \leq 2500\,\mu m$), consistent with many experimental observations. The exception is the dip in the variation of $\overline{f}_v$ with $Sc^{1/3}\ Re^{1/2}$ in the data set of Kinzer and Gunn (1951), which was attributed to experimental inaccuracies in their experimental set up by later studies. In Figure 8.16a, the product $Sc^{1/3}Re^{1/2}$ has also been converted into an equivalent drop radius r_{eq}, which denotes the radius of an equivalent sphere of the same mass. For $Sc^{1/3}\ Re^{1/2} \leq 1.4$, that is, drops with $r_{eq} < 60\,\mu m$, $\overline{f}_v$ approaches 1 asymptotically (Figure 8.16b). Overall, we note from Figure 8.16 that $\overline{f}_v$ is approximately 9.5 for a raindrop with $r_{eq} = 1\,mm$, and 15 for a raindrop with $r_{eq} = 2\,mm$. Thus, the evaporation of a 1 mm raindrop, falling at its terminal velocity in air, proceeds approximately 10 times faster than the evaporation of a drop of the same size at rest. Consequently, calculating the evaporation rate of raindrops on the basis of eq. (8.23) is a considerable underestimation.

For rain to reach the surface, RH_w below a cloud needs to be high enough that the raindrops do not evaporate completely on their way to the surface. In fact, not all precipitation reaches the ground; some evaporates as it falls. The evaporation of raindrops can be observed in the form of virgae (Figure 1.8). As an example, virgae have been observed in 30–51 % of all stratocumulus clouds over the South Atlantic (Dzambo et al., 2019).

8.3.2 Maximum Raindrop Size

Raindrops are limited to 3–5 mm in equivalent radius (Hobbs and Rangno, 2004; Gatlin et al., 2015; Loftus and Wordsworth, 2021) because the chance of disruption increases with size. Break-up can occur because the aerodynamically induced circulation that develops inside the drop becomes large enough to overcome the surface tension force (Chapter 7). Surface tension can be imagined as a force acting in the plane of the surface, trying to minimize the droplet surface area by keeping it in a spherical shape (Figure 7.3).

The maximum raindrop radius r_{max} can be calculated by equating the drag force (eq. 8.37) and the surface tension force:

$$\frac{\pi}{2} r_{max}^2 v_T^2 \rho_a C_D = 2\pi r_{max} \sigma_{w,a}. \tag{8.63}$$

https://doi.org/10.1017/9781009485654.009 Published online by Cambridge University Press

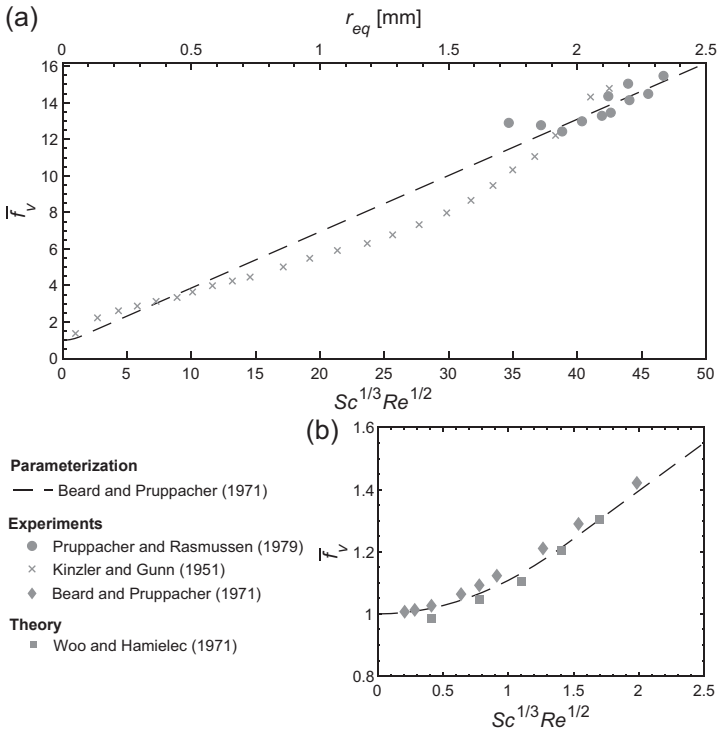


Figure 8.16 Mean ventilation coefficient $\overline{f}_v$ as a function of the product of Reynolds number Re and the Schmidt number Sc. Markers denote measurements of Kinzer and Gunn (1951), Beard and Pruppacher (1971), and Pruppacher and Rasmussen (1979). Also shown are solutions from numerically solving the convective diffusion equation by Woo and Hamielec (1971). The solid and dashed lines correspond to empirical expressions for $\overline{f}_v$ taken from Beard and Pruppacher (1971) (eqs. 8.61 and 8.62). Also indicated is an approximate equivalent raindrop radius r_{eq}, obtained by inserting eq. (8.39) into eq. (8.62), using a constant $Sc = 0.71$ (applicable to the experimental conditions), and assuming a constant $v_T = 9.87\,\mathrm{m\,s^{-1}}$.

Solving for r_{max} yields

$$r_{max} = \frac{4\sigma_{w,a}}{C_D \rho_a v_T^2}. \tag{8.64}$$

The drag coefficient in eq. (8.64) is generally unknown because it depends on v_T, as noted earlier. Here, we approximate it by $C_D = 0.8$. This value lies between $C_D = 0.45$ for a perfect sphere (eq. 8.44) and $C_D = 1.17$ for a disk at $Re > 1000$ (Hoerner, 1965), owing to the oblate shape of raindrops (Figures 8.11 and 8.12). We then take the maximum terminal velocity $v_T = 9\,\mathrm{m\,s^{-1}}$ from Figure 8.12, and use characteristic environmental conditions of $p = 800\,\mathrm{hPa}$ and $T = 278\,\mathrm{K}$, which subsequently lead to the following values for the air density: $\rho_a = 1\,\mathrm{kg\,m^{-3}}$ and for the surface tension of the air–water interface: $\sigma_{w,a} = 0.075\,\mathrm{N\,m^{-1}}$ (Table 9.1). Upon

https://doi.org/10.1017/9781009485654.009 Published online by Cambridge University Press

combining all these values, we ultimately arrive at $r_{max} = 4.6\,\text{mm}$. In most cases, however, raindrop break-up is induced by the collisions of a raindrop with smaller droplets.

8.3.3 Conditions Leading to Raindrop Break-up

In a collision where both the collector drop (drizzle) and the collected droplet are smaller than 100 μm, the coalescence efficiency $\hat{E}$ can be assumed to be one (Beard and Ochs, 1995). This no longer holds true if one or both of the colliding hydrometeors become considerably larger than 100 μm. As shown in Figure 8.17b, in this case, $\hat{E} < 1$ and $\hat{E}$ decreases with increasing raindrop size. Moreover, $\hat{E}$ is smaller for similar sized raindrops.

If two drops collide and coalescence occurs, the total energy of coalescence E_{coal}, which the resulting drop gains due to collision–coalescence, must be either dissipated or used to form new surfaces. It is given as

$$E_{coal} = E_{CKE} + \Delta E_{sfc}, \tag{8.65}$$

where all energies are given in units of J. E_{CKE} is the collision kinetic energy, and ΔE_{sfc} denotes the change in surface energy.

E_{CKE} is the amount of energy that the newly formed drop obtains from the kinetic energy of the colliding drop pair. It depends on the kinetic energies of the two drops before their collision and is given as (Low and List, 1982):

$$E_{CKE} = \left(\frac{2}{3}\pi\rho_l\right)\frac{R^3}{1+(R/r)^3}v_r^2, \tag{8.66}$$

where

$$v_r = v_T(R) - v_T(r), \tag{8.67}$$

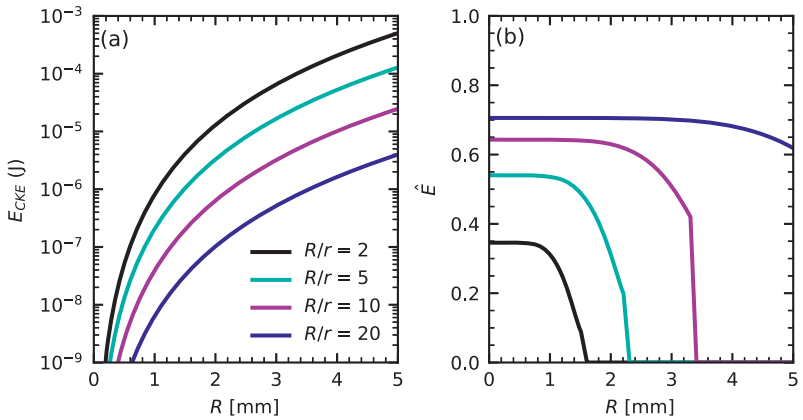


Figure 8.17 (a) E_{CKE} (J) as a function of the larger collector drop radius R (mm) for four different values of the radius ratios of colliding hydrometeors, R/r, using eq. (8.66). (b) Empirical coalescence efficiency $\hat{E}$ as a function of R for four different values of R/r, using eq. (8.70).

https://doi.org/10.1017/9781009485654.009 Published online by Cambridge University Press

is the relative velocity of impact, which is given by the difference in terminal velocities between the collector drop and the droplet with which it collides. Further, R/r is the ratio of the radius of the larger raindrop R to the radius of the smaller droplet r.

The surface energy term ΔE_{sfc} describes the energy that the newly formed drop gains due to the reduction in the total surface area (which releases energy). It is given by

$$\Delta E_{sfc} = 4\pi\sigma_{w,a}(r^2 + R^2) - E_{sfc,n}, \tag{8.68}$$

where $E_{sfc,n}$ is the surface energy of the equivalent sphere for the new drop:

$$E_{sfc,n} = 4\pi\sigma_{w,a}(r^3 + R^3)^{2/3}. \tag{8.69}$$

Since a collision between drops is not an elastic collision, in which kinetic energy would be conserved, some of the kinetic energy of the colliding drops must be dissipated by circulation inside the raindrop. If the dissipation of energy is insufficient, raindrop break-up will occur. Values of E_{CKE} or ΔE_{sfc} can be obtained from wind tunnel measurements, where differently sized droplets can be collided under controlled conditions (e.g., Szakáll and Urbich, 2018). An empirical coalescence efficiency $\hat{E}$ based on the total energy of coalescence E_{coal} was derived by Low and List (1982) from experimental data obtained in a wind tunnel as:

$$\begin{aligned} \hat{E} &= a\left(\frac{R/r}{R/r+1}\right)^2 \exp\left(-\frac{b\sigma_{w,a}E_{coal}^2}{E_{sfc,n}}\right), \quad \text{for } E_{coal} < 5\,\mu\text{J}, \\ &= 0, \quad \text{for } E_{coal} \geq 5\,\mu\text{J}. \end{aligned} \tag{8.70}$$

Here, $\sigma_{w,a}$ is the surface tension of the air–water interface, $a = 0.778$, and $b = 2.61 \times 10^6\ \text{J}^{-2}\,\text{m}^2$. E_{CKE} and the empirical coalescence efficiency $\hat{E}$ are shown for four different values of R/r in Figure 8.17. As can be seen, E_{CKE} increases rapidly with increasing R and with decreasing R/r. At the same time, $\hat{E}$ decreases with increasing R and hence increasing E_{CKE}, thus increasing the probability of break-up. As shown in Figure 8.17b, $\hat{E}$ drops to zero ensuring break-up when E_{coal} is equal to or exceeds 5 μJ. This occurs, for instance, when the radius of the large raindrop is 1.5 mm and that of the smaller raindrop is 0.75 mm ($R/r = 2$) or when the size of the raindrop is larger than 3.5 mm in radius, and the colliding drop is larger than 0.35 mm ($R/r \leq 10$).

In summary, for cloud droplets the collision efficiency is found to be $E \leq 1$ due to aerodynamic interactions of the surrounding air with the different droplets, but the coalescence efficiency $\hat{E} \approx 1$. Therefore, the collection efficiency approximately equals the collision efficiency: $\tilde{E} \approx E$ (eq. 8.35). For raindrops, the opposite is true: The collision efficiency $E \approx 1$, but the coalescence efficiency is $\hat{E} < 1$ due to break-up, so that the collection efficiency approximately equals the coalescence efficiency: $\tilde{E} \approx \hat{E}$.

8.3.4 Types of Raindrop Break-up

During moderate to heavy rainfall conditions, there are about 1 to 10 hydrometeor collisions per second in 1 m^3 of air (Beard et al., 1983). Collisions that do not lead to permanent coalescence were found to often produce multiple small so-called satellite drops with radii of 20–220 μm (Brazier-Smith et al., 1973). The number of satellite drops increases with the

https://doi.org/10.1017/9781009485654.009 Published online by Cambridge University Press

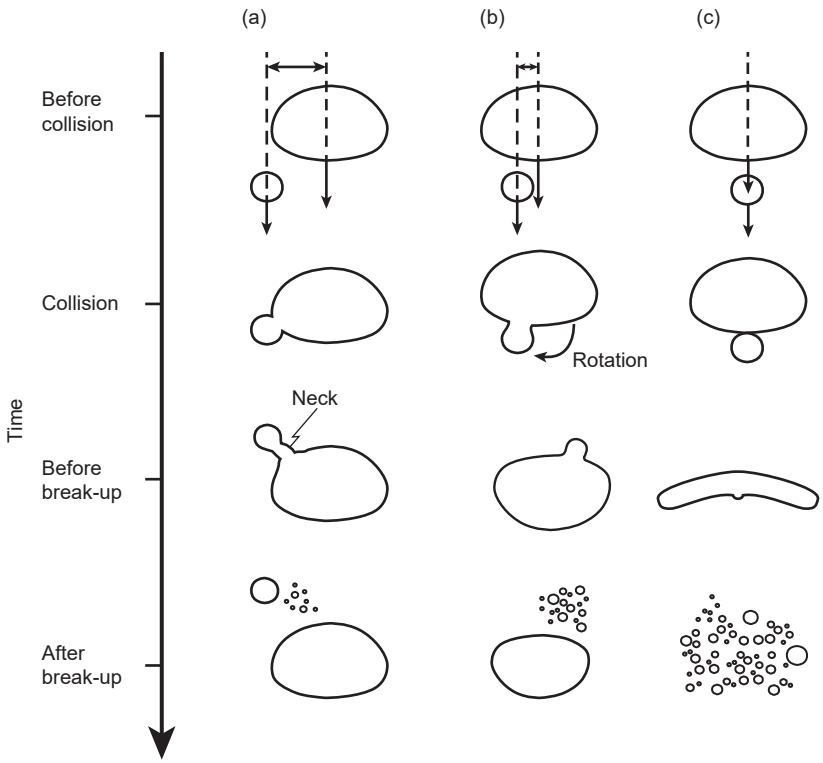


Figure 8.18 Schematic illustration of the three common types of raindrop break-up: (a) neck or filament break-up, (b) sheet break-up, and (c) disk break-up.

increasing size of the large drop and depends on the type of break-up (Emersic and Connolly, 2011). Low and List (1982) found three different types of raindrop break-up, namely neck or filament break-up, sheet break-up, and disk break-up, as schematically shown in Figure 8.18.

Neck or filament break-up (Figure 8.18a) is caused by grazing collisions, that is, the impact is at the edge of the larger drop. It produces a spinning, elongated drop which may quickly tear apart. Up to 10 satellite drops are created by the disintegration of the connecting neck (Emersic and Connolly, 2011). The identities of the two colliding drops are preserved. This break-up form produces the smallest total surface area and hence needs the least E_{CKE}.

Sheet break-up (Figure 8.18b) occurs when drops collide in such a way that one side of the large drop is torn off, with the point of impact between the edge and the center of the large drop. The bulk of the large drop then rotates about the point of impact, issuing a sheet of water that breaks apart into satellite drops. During sheet break-up, only the identity of the large drop is preserved. Sheet break-up was found to produce up to 24 satellite drops when the large drop approached $r = 3$ mm (Emersic and Connolly, 2011).

For disk break-up (Figure 8.18c), the point of impact is close to the center of the larger drop. Coalescence occurs temporarily, but the disk that forms upon impact disintegrates into a large number of small satellite drops. This break-up form is associated with the formation of the

https://doi.org/10.1017/9781009485654.009 Published online by Cambridge University Press

largest total surface area (Low and List, 1982) because E_{CKE} is highest. The original identities of the drops are lost.

To summarize, break-up is important in limiting the growth of the largest drops and is the reason why raindrops rarely exceed 5 mm in radius (Hobbs and Rangno, 2004; Gatlin et al., 2015; Loftus and Wordsworth, 2021). The consequences of raindrop break-up for the raindrop size distribution will be discussed in Chapter 10.

8.3.5 Summary of Processes in a Warm Cloud

Prominent locations of considerable amounts of warm rain are islands like Hawaii, where the collision–coalescence process is sped up due to orographic forcing (Qin and Fu, 2016). The growth processes in such a cloud are summarized in Figure 8.19, illustrating a warm convective cloud, that is, a cloud where water is present only in the liquid phase and where the ice phase is absent.

In such a cloud, aerosol particles initially take up water by hygroscopic growth, leading to the formation of aqueous solution droplets. These solution droplets then activate into cloud droplets (Chapter 7). The cloud droplets subsequently increase in size by condensational growth until some droplets are large enough to overcome the growth gap (Figure 8.7). Then

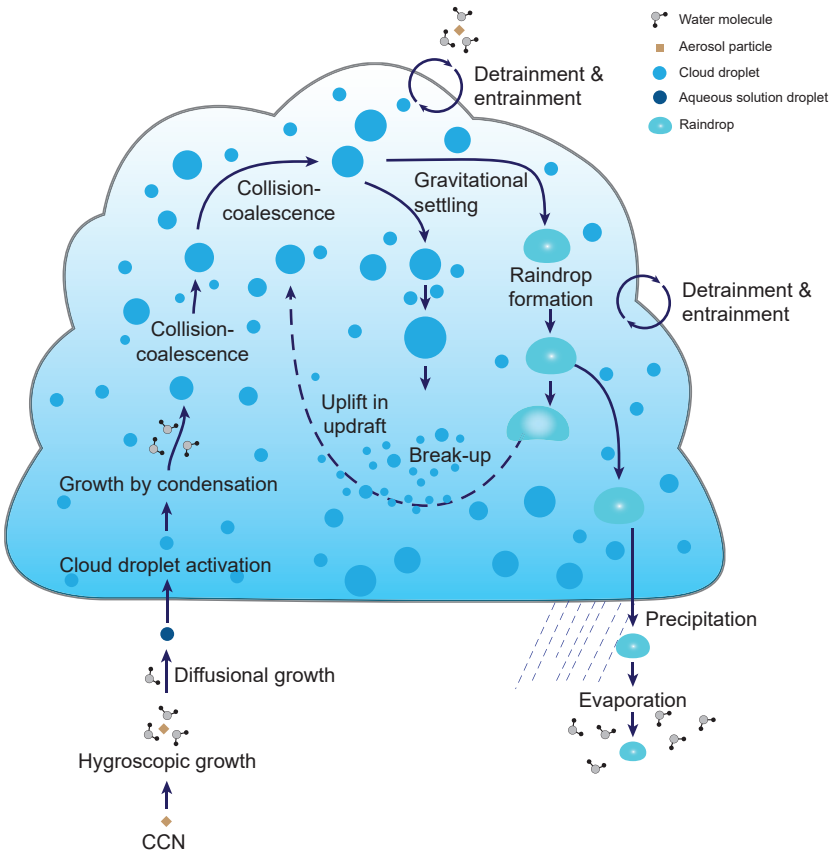


Figure 8.19 Microphysical processes occurring in a convective cloud in the absence of an ice phase. The small arrows show typical trajectories of the temporal evolution of cloud particles.

https://doi.org/10.1017/9781009485654.009 Published online by Cambridge University Press

growth by collision–coalescence becomes more efficient than condensational growth forming drizzle and raindrops. These either leave the cloud intact or break-up upon collisions with cloud droplets and drizzle drops if the raindrops are larger than 5 mm in radius, ejecting satellite droplets. These satellite droplets may be carried up again in the cloud if they find themselves in a region of updraft. Below cloud base, raindrops may partly or fully evaporate depending on the relative humidity below cloud base and on their size. This increases the relative humidity below cloud base until it is sufficiently high that raindrops do not fully evaporate any longer and eventually reach the ground as precipitation.

https://doi.org/10.1017/9781009485654.009 Published online by Cambridge University Press